Int J Adv Manuf Technol (2016) 85:1687–1712
DOI 10.1007/s00170-015-8071-5

ORIGINAL ARTICLE

Critical analysis of friction stir-based manufacturing processes

Mustafa Kemal Kulekci[1] · **Ugur Esme**[1] · **Baris Buldum**[1]

Received: 15 December 2014 / Accepted: 2 November 2015 / Published online: 12 November 2015
© Springer-Verlag London 2015

Abstract In this study, a detailed analysis of friction stir-based processes that can significantly contribute to joining of materials and surface property enhancement has been completed. Past, present, and future projections, advantages and disadvantages, technological barriers, and drawbacks of these processes have been given. Detailed explanations of the recent developments of friction stir-based processes and main components are given. Potential industrial applications have been assessed and evaluated using economic and technological considerations. In industrial applications, friction stir-based processes can be used in conjunction with additive processes such as laser-engineered near net shaping, thermal spraying and laser-assisted direct metal deposition processes. Developments in friction stir-based processes have led to improved metallurgical and mechanical properties such as microstructure modification, refinement, homogenization, surface cladding, corrosion, fatigue, wear, and hardness of metallic materials. The results of the study conclusively predict that reasonable costs and improved properties of processed materials will lead to a substantial increase in the use of friction stir-based processes.

Keywords Friction stir welding · FSW · Friction stir processing · Friction stir hardening · Riveting · Microstructure modification · Friction stir channeling · Hybrid processing · Hybrid manufacturing

✉ Mustafa Kemal Kulekci
mkkulekci@mersin.edu.tr

[1] Institute of Applied and Natural Sciences, Faculty of Tarsus Technology, Mechanical and Manufacturing Engineering Department, Mersin University, 33480 Tarsus, Mersin, Turkey

1 Introduction

Friction stir-based processes are used for processing aluminum [1–3], copper [4], magnesium [5], brass [6], plastics [7], and steel [8] based materials. Since the invention of friction stir welding (FSW) process in 1991, many new friction stir-based processes have been derived from the basic FSW process and they have been successfully adapted to industrial applications [1, 2]. Friction stir-based industrial processes are given in Fig. 1. Friction stir-based processes cause intense plastic deformation, material mixing, and thermal exposure resulting in significant microstructural refinement, densification, and homogeneity of the processed zone [1, 2]. Friction stir-based processes can be used for surface modification and control of microstructure near-surface layer, surface hardening, joining-bonding of metallic materials, surface cladding, composite layer manufacturing, and friction stir channeling [10–14]. The potential application areas of these processes are in marine, aerospace, rail, and automotive industries [15–18].

In this study, a detail analysis of friction stir-based processes has been completed. Past, present, and future projections, advantages, disadvantages, technological barriers, and drawbacks of the processes have been given. In addition, potential industrial applications have been assessed and evaluated using economic and technological results.

2 Friction stir joining

2.1 Friction stir welding

The principal features of FSW are shown in Fig. 2a. The process is repeatable, can be easily monitored, and does not pose safety hazards, such as fume or radiation [20–23]. The FSW

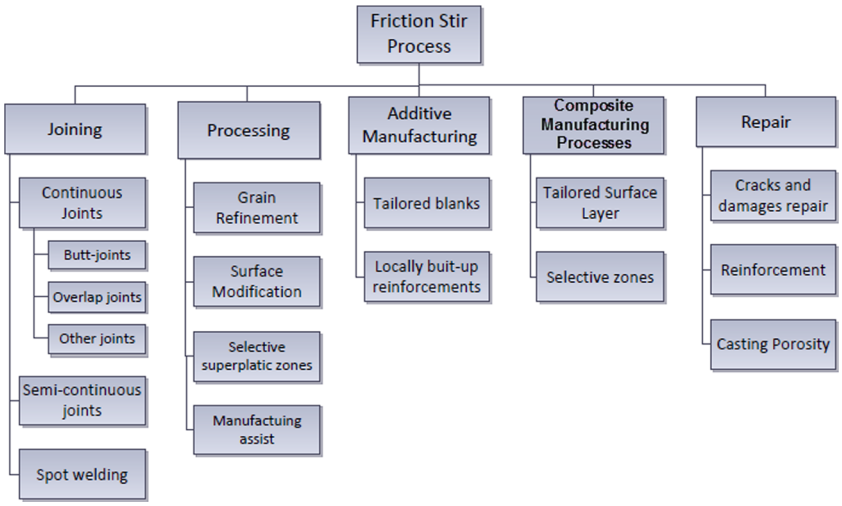

Fig. 1 Friction stir processing applications and developments [9]

tool is generally made up of a profiled pin (or probe) which projects out of a shoulder with a larger diameter, as seen in Fig. 2a. The specifically profiled probe makes initial contact as it is plunged into the region that is to join or to be processed. The components to be welded are secured to prevent the butted joint faces from being forced apart as the probe passes through and along the seam. For welding of thicker plates (25–50 mm thick), usually, a pilot hole of smaller diameter than the probe is typically drilled at the start to assist the plunging operation [24–27]. The depth of penetration is controlled by the length of probe below the shoulder of the tool. The frictional heat generated during initial plunging heats the adjacent metal around the probe as well as a small region of material underneath the probe. In addition, the contacting shoulder prevents highly plasticized material from being expelled from the welding region [27, 28]. Thermally softened and heat-affected zone take up a shape corresponding to that of the overall tool geometry [19, 29–32]. The heat-affected zone is much wider at the top surface (in contact with the shoulder) and tapers down while the probe diameter reduces, as seen in Fig. 2b [33–39]. The combined frictional heat from the probe and the shoulder creates a highly plasticized "third body" condition around the immersed probe and the adjacent contacting surface of workpiece. This highly plasticized material provides for some hydrostatic effect as the rotating tool moves along the joint, which helps the plasticized material to flow around the tool [40–43].

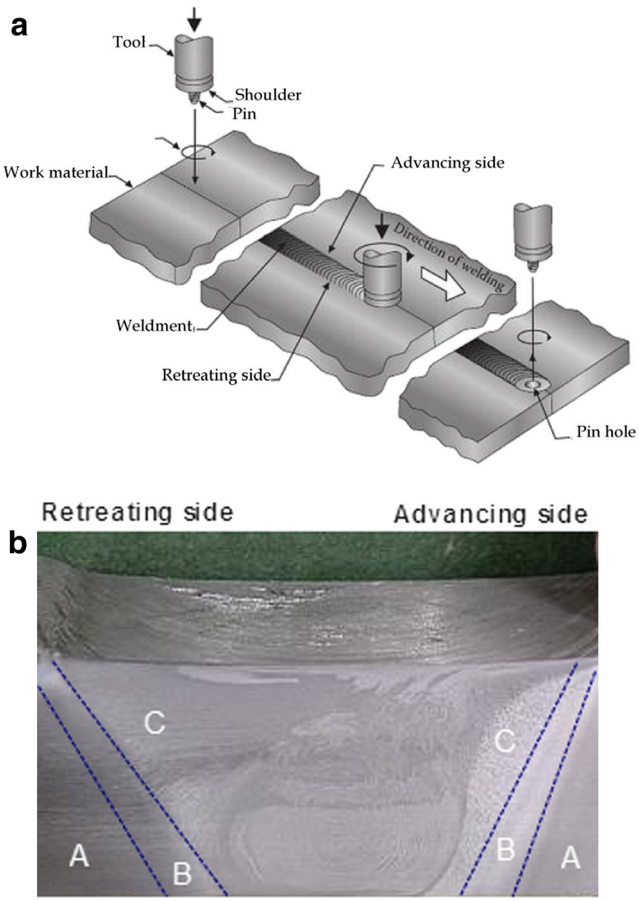

Fig. 2 **a** Schematic illustration of friction stir welding [2, 19]. **b** Microstructural zone classification in a friction stir weld, the left side is the 7050, the right side is the 2024, which is the advancing side of the weld (*A*: parent material, unaffected by the process; *B*: HAZ, thermally affected but with no visible plastic deformation; *C*: TMAZ, affected by heat and plastic deformation) [3]

The plasticized weld material then coalesces behind the tool as the tool moves away. For butt joining the length of the pin approximates to the thickness of the workpiece if the weld is done from one side. For double-sided weld, the length of pin is approximately equal to half of the workpiece thickness [41, 44–46]. The pin is traversed through the joint line while the shoulder is in intimate contact with the top surface of the workpiece to avoid expelling softened material. The FSW tools are manufactured from a wear-resistant material with good static and dynamic properties at elevated temperature [15–18]. A properly designed FSW tool permits up to 1000 m of weld to be produced in 5-mm-thick aluminum

extrusions without changing the tool [23, 27, 28]. The onion ring-like structure of the nugget is high-quality stir weld, in which no porosity or internal voids are detectable, as seen in Fig. 2b. In macrosections of good quality welds, the nugget is visible at the center of the weld. Outside of the nugget, there is a thermo mechanically affected zone, which has been plastically deformed and shows some areas of partial grain refinement [9, 10, 47–49]. The comparison of tensile test results of base metal, FSW, and metal inert gas (MIG) joints is given in Fig. 3. As seen in the figure, the tensile test strengths of FSW, MIG weld, and base metal (BM) are 177.5, 163, and 86.4 MPa, respectively. Tensile strength of FSW was 3 % lower than BM. On the other hand, strength decrease was about 51.3 % in MIG welded specimens. The results of the tensile tests show that 88 % strength improvement can be obtained by the FSW process when compared with MIG. The tensile strength of the FSW joint is stronger than the MIG joint, but lower than the base metal, as seen in Fig. 3. This strength improvement can be explained by the structure obtained by the FSW process. The microstructure of FSW is a refined structure, while MIG welds have a cast structure [27].

2.1.1 Formability of FSW joints

The stirring effect of the FSW process gives a finer microstructure to the weld whereas the MIG welding process gives a coarser columnar crystalline structure [31, 32]. The stirring effect and refined structure improve the mechanical properties of the FSW joint. Elongation results of FSW, MIG joints, and base metal obtained from tensile test are given in Fig. 3. FSW joints have better formability characteristics than MIG, as seen in Fig. 3. Formability of the metallic materials is characterized by elongation obtained by tensile test. The elongation values are 16, 14, and 4 for base, FSW, and MIG welded specimens, respectively, as seen in Fig. 3. This situation can be explained by the solid-state nature of the FSW process that results in refined microstructure rather than a cast structure. Higher heat intensity in the liquid phase welding processes such as MIG deteriorates the mechanical properties of the joints. Better mechanical properties can be obtained by FSW than the conventional MIG process [27]. One of the major potential application areas for friction stir welding is the tailor-welded blank (TWB). The TWB consists of various sections of flat sheet, which are abutted and then joined together. These joined flat sheets then enter a forming operation to shape the joined sheets into their final geometry. At this stage, formability characteristic of weld seam is important. FSW has better formability than liquid phase welding process, as seen in Fig. 3. The purpose of the TWB is to optimize material utilization, not only for improved material utilization, but also for reducing the weight of the final formed component. These tailor-welded blanks often have variations in material thickness across the joint line. To join the blanks that have variations in material thickness, a dissimilar thickness butt weld is required. Hardness variation and distribution of FSW and MIG welded specimens on the surface of the weld and cross-section are shown in Fig. 4. The thermal cycles generated during FSW welding affect the microstructure of metallic materials. Hardening precipitates can suffer three phenomena during the thermal cycles: dissolution, growth, and coalescence [50]. These phenomena cause a decrease in the mechanical strength of the material in different parts of the welded joint and create a minimum hardness zone (MHZ), which controls the mechanical properties of the weld.

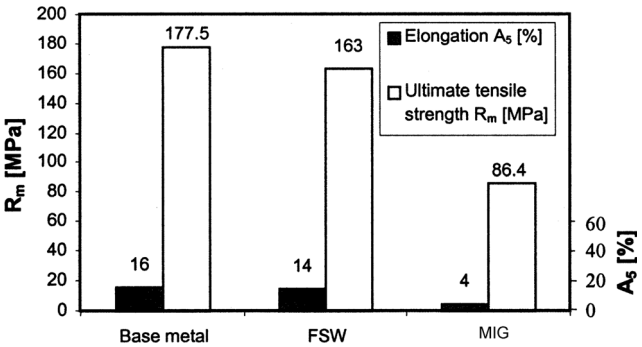

Fig. 3 Comparison of formability of FSW, MIG and base metal (FSW: friction stir welding, MIG: metal inert gas, arc welding, base metal: EN AW-2014 (AlCu4SiMg) aluminum alloy) [27]

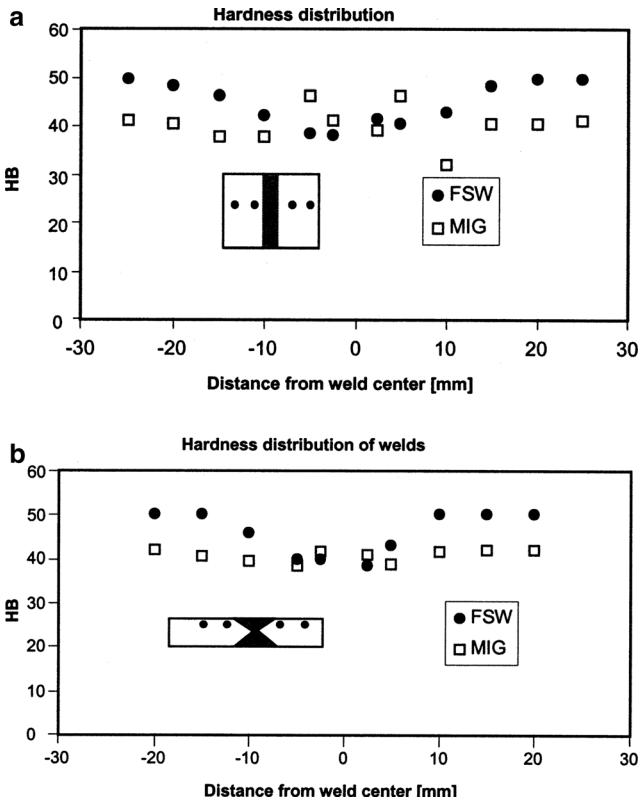

Fig. 4 Hardness variation and distribution of FSW and MIG welded specimens on the surface of weld (**a**) and cross section (**b**) [27]

Figure 4 shows that the region where hardness decreases is narrower for FSW than MIG weld. Heat-affected zone of FSW is narrower than the MIG welded joints. The difference between the width of hardness reduction regions of the FSW and MIG joints can be explained by the fact that the welding temperature of FSW is about 480 °C [27], far lower than that of the MIG process.

The limiting dome height (LDH) test is used for formability of sheet metal alloy. Miles et al. [51] investigated the formability of FSW and gas tungsten arc welded (GTAW) joints comparing the results of tensile and limiting dome height (LDH) test. Hardness profile and tensile test data of FSW and GTAW are shown in Fig. 5. For the 5182-O and the 5754-O alloys, there were no significant differences in any of the average tensile properties of the FSW and GTAW samples at the 95 pct confidence level. For 6022-T4, the yield strength and ultimate tensile strength drops significantly in the welded specimens, although the FSW specimens retain more strength than the GTAW specimens. In addition, the FSW samples had a greater average elongation than the GTAW samples, by about 50 pct. The fracture location was always in the HAZ for the FSW samples, while it was always in the weld for the GTAW samples. This can be explained by looking at tensile data given in Fig. 5, where the softening in the gas tungsten arc welding case is seen to be much greater than in the friction stir welding case. The average tensile properties for the FSW samples are more consistent than those of the GTAW samples, particularly in the case of alloy 6022-T4. While the variance in the yield strengths are similar, the ultimate tensile strength, uniform elongation, and total elongation for the FSW specimens are significantly less than those of the GTAW specimens. The LDH results are shown in Fig. 6. 5xxx series alloys perform about the same regardless of the welding process used, while the 6022-T4 has a lower LDH for gas tungsten arc welding than for friction stir welding. The FSW specimens failed in the HAZ and not in the weld for the LDH test, but several of the GTAW samples failed in the weld. Full-dome LDH test causes stretching both along and across the weld [52]. The strain applied across the weld and the HAZ causes deformation to localize in this softened region by creating a fracture parallel to the weld (or in the weld for some GTAW specimens), as seen in Fig. 6. The friction stir welding process results in about the same average formability (as measured by both tensile elongation and formability testing) as the gas tungsten arc welding process for the 5182-O and 5754-O welded sheets, but with slightly more consistent properties. For the 6022-T4 alloy, friction stir welding provides better ductility than gas tungsten arc welding because it causes less softening in the HAZ, as seen in the microhardness results. However, its advantage depends on the deformation mode imposed. When tensile stretch conditions (with the weld transverse to the tensile axis) or biaxial stretch conditions were imposed on the weld, the FSW samples performed better than GTAW samples. When a plane-strain deformation condition was imposed (with the weld along the major axis), FSW samples did not have much advantage [52].

Silva et al. [53] investigated the single point incremental forming (SPIF) of tailored blanks produced by friction stir welding [53]. The authors evaluated the formability of the TWB by means of benchmark tests carried out on truncated conical and pyramidal shapes, as seen in Fig. 7. Results of the study show that the combination of SPIF with tailored welded blanks produced by FSW seems promising in the manufacture of complex sheet metal parts with high depths [53]. As can be

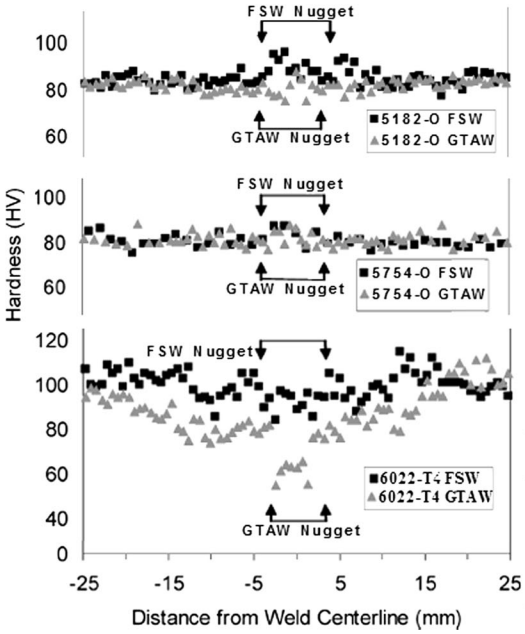

Tensile Data for Base and Welded 5182-O Sheets

Weld Type	0.2 Pct Yield (MPa)	UTS* (MPa)	Elongation at UTS	Total Elongation	Fracture Location B = Base H = HAZ, W = Weld	Number of Samples
Base	131.0	285.4	25.3 pct	27.3 pct	N/A	15
Standart deviation	2.2	3.3	0.1 pct	0.7 pct	-	-
FSW	138.2	285.7	23.3 pct	25.7 pct	B = 100 pct	15
Standart deviation	4.6	1.7	0.1 pct	0.7 pct	-	-
GTAW	127.4	283.2	24.9 pct	27.0 pct	B = 100 pct	15
Standart deviation	5.5	2.1	0.2 pct	1.0 pct	-	-

Tensile Data for Base and Welded 5754-O Sheets

Weld Type	0.2 Pct Yield (MPa)	UTS* (MPa)	Elongation at UTS	Total Elongation	Fracture Location B = Base H = HAZ, W = Weld	Number of Samples
Base	94.4	236.3	24.6 pct	26.5 pct	N/A	15
Standart deviation	4.3	5.6	1.5 pct	1.0 pct	-	-
FSW	98.1	235.6	22.7 pct	24.9 pct	B = 100 pct	15
Standart deviation	6.3	2.5	1.0 pct	0.8 pct	-	-
GTAW	96.6	235.5	22.1 pct	24.1 pct	B = 100 pct	15
Standart deviation	2.0	5.6	1.7 pct	2.0 pct	-	-

Tensile Data for Base and Welded 6022-T4 Sheets

Weld Type	0.2 Pct Yield (MPa)	UTS* (MPa)	Elongation at UTS	Total Elongation	Fracture Location B = Base H = HAZ, W = Weld	Number of Samples
Base	163.6	263.3	26.3 pct	29.6 pct	N/A	15
Standart deviation	1.9	1.2	1.0 pct	1.0 pct	-	-
FSW	140.1	235.0	12.3 pct	12.9 pct	H= 100 pct	15
Standart deviation	4.7	4.7	0.4 pct	0.6 pct	-	-
GTAW	19.7	207.4	7.7 pct	8.2 pct	W= 100 pct	15
Standart deviation	5.2	14.7	1.7 pct	1.8 pct	-	-

*UTS - ultimate tensile strength.

Fig. 5 Hardness, yield, UTS, and elongation results of base, FSW, and GTAW [51]

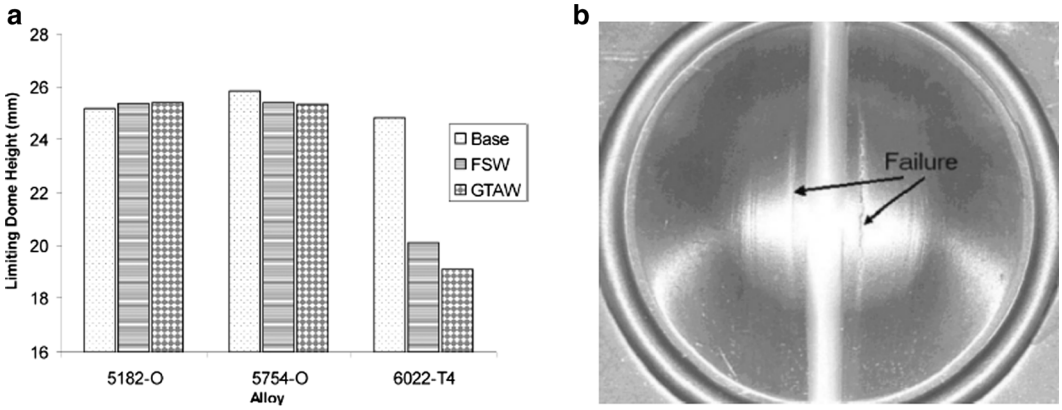

Fig. 6 **a** LDH test results for three alloys using base sheets, FSW sheets, and GTAW sheets. **b** Failure in alloy 6022-T4 during full dome LDH tests occurred in the HAZ, on either side of the weld, for all of the FSW specimens. For GTAW specimens, many of the failures occurred in the weld [51]

seen in Fig. 7, the final quality of the sheet metal parts is greatly dependent on the quality of the welding joint produced by friction stir welding. On one hand, it is possible to SPIF friction stir-based TWB parts with high-forming depths, similar to those obtained with conventional reference blanks of the same material, in which fracture develops outside the welding joint (Fig. 7a). On the other hand, it is also possible to obtain bad SPIF parts where cracking occurs prematurely in

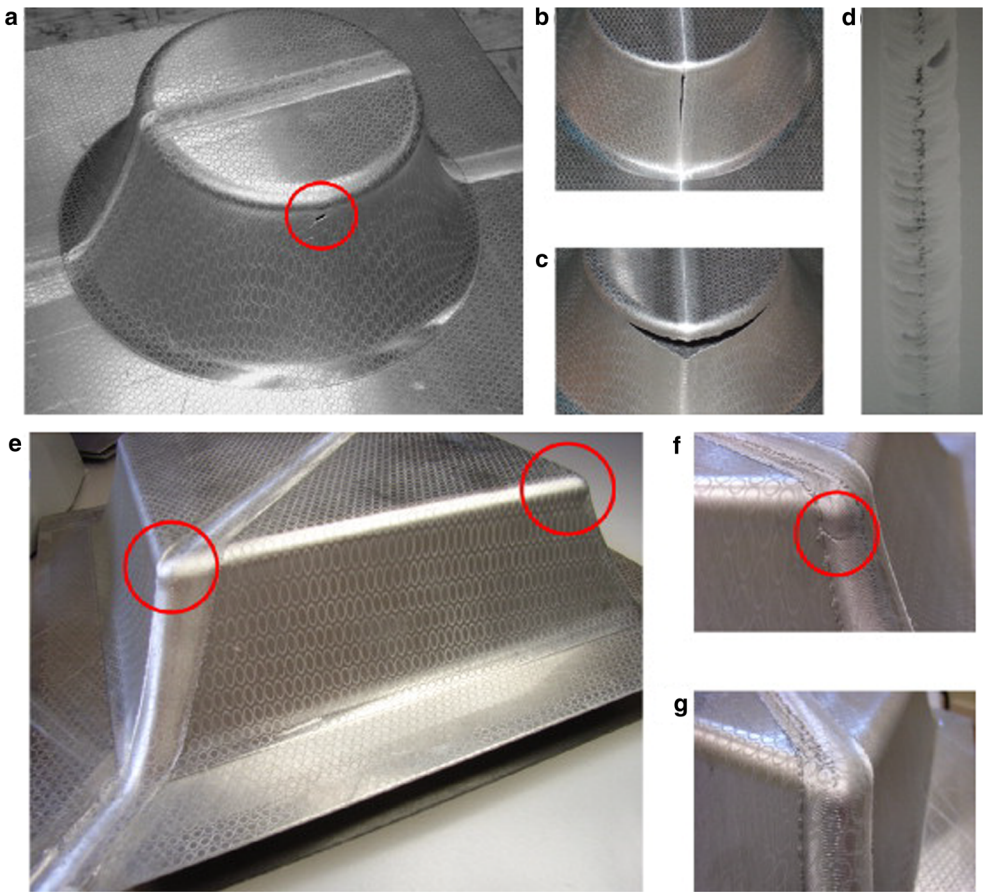

Fig. 7 Truncated conical and pyramid benchmark formability parts produced from TWB of Aluminium AA1050-H111 sheets. **a** Good formability showing a crack outside the welding joint (TWB with a uniform 2.0 mm thickness profile). **b** Low formability showing necking and subsequent cracking along the welding joint (TWB with a uniform 1.5 mm thickness profile). **c** Low formability derived from a crack triggered in the welding joint (TMAZ) and subsequently propagated along the circumferential direction perpendicular to the welding joint (TWB with a uniform 1.5 mm thickness profile). **d** Detail of an X-ray of a welding joint showing several defects (TWB with a uniform 1.5 mm thickness profile). **e** Cracks are triggered almost simultaneously at the corners with and without welding joints. **b** Detail of **e** showing the crack at the corner. **f** Detail of the corner placed in the opposite diagonal to **g** showing no evidence of cracking in the welding joint [53]

the welding joint (Fig. 7b, c). This leads to the conclusion that SPIF of FSW tailored blanks is capable of producing industrial sheet metal parts with high-forming depths if a good quality control of the welding joints is ensured. Application of non-destructive methods based on X-ray (Fig. 7d), ultrasonic, and liquid penetration testing is crucial for the identification of possible welding defects that may diminish the overall formability of SPIF. Results show that a significant part of the formability problems occurred with TWB having a uniform 1.5 mm thickness profile. Possible explanation for this is twofold and can be attributed to (i) the difficulties of the FSW experimental setup utilized by the authors for welding sheet metal blanks equal to or below 1.5 mm thickness and to (ii) inherent difficulties of FSW for joining sheet metal blanks with small thicknesses due to the fact that material flow around the cylindrical rotational welding tool progressively drifts from 3D to 2D as the thickness of the sheets to be welded is reduced. Figure 7e, f shows a truncated pyramid SPIF part produced from a TWB made of Aluminium AA1050-H111 with a uniform 2.0 mm thickness profile. The welding joint is parallel to the rolling direction and is positioned across the corners of the SPIF part in order to evaluate the performance of the TWB in severe forming conditions. As can be seen, cracks are triggered almost simultaneously at the corners with and without welding seam that are marked in the figure (refer also to the detail included in Fig. 7b). This result together with the detail included in Fig. 7g showing a sound welding seam, with no evidence of cracking, at the corner placed in the opposite diagonal further confirms the very good forming potential of the tailored blanks produced by FSW [53].

2.1.2 Fatigue behaviour of FSW joints

The parameters of FSW influence fatigue behavior of FSW joints [23]. Results of studies conclude that a parameter optimization is needed to obtain better fatigue performance of FSW joint, as seen in Fig. 8. In this study, a better fatigue strength had been obtained with minimum pin diameter and minimum tool rotation while other parameters held fixed. The experimental data given in Fig. 8 indicate that increasing tool rotation for a fixed tool pin diameter reduces fatigue strength of FSW joints. Increasing the tool pin diameter for a fixed tool rotation decreases fatigue strength.

2.2 Friction stir spot welding

The friction stir spot welding (FSSW) is a process that has brought notable improvements to the light construction industry [54, 55]. The importance of FSSW depends not only on the process parameters (geometry, position, rotation of the tool, dwell time, plunging depth, and force applied to the tool), but also on the nature of the material. The FSSW process consists of plunging, stirring, and drawing out phases, as seen in Fig. 9a. The process starts with a tool rotation then a slow plunging inside the material is carried out, compressing a pin in a spot before the shoulder gets in touch with the upper surface of the workpiece [56]. Afterwards, the stirring phase allows for mixing together of the materials of the two pieces. Finally, after reaching the desired plunging, the process stops and the tool is drawn out. When the tool plunges inside the sheet metal, the material interface undergoes a bending that is afterwards eliminated by the effect of the cutting efforts generated around the pin [54]. Material flow behavior during FSSW is given in Fig. 9b. When the welding is executed with a threaded pin, the material under the shoulder shows a movement towards the pin base direction (1), then spiral-shaped along the pin surface towards the bottom as a result of the direction of the dragging force of the rotation (2). Once the extremity of the pin is reached, the material is forced towards the top and outside, then it comes back to the pin direction in accordance with the helical rotation (3) [54]. The material transport process is repeated as the distance from the pin grows, thus creating a stirring zone. It has been demonstrated

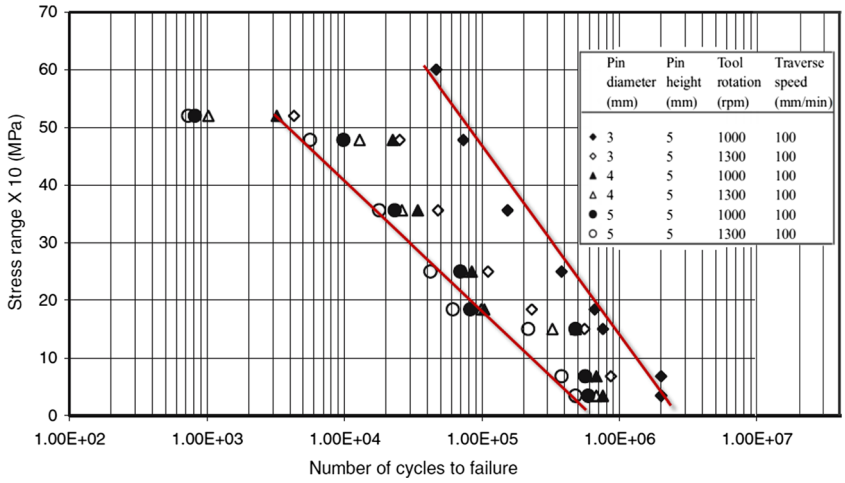

Fig. 8 The fatigue behavior of FSW joints obtained with different parameter [23]

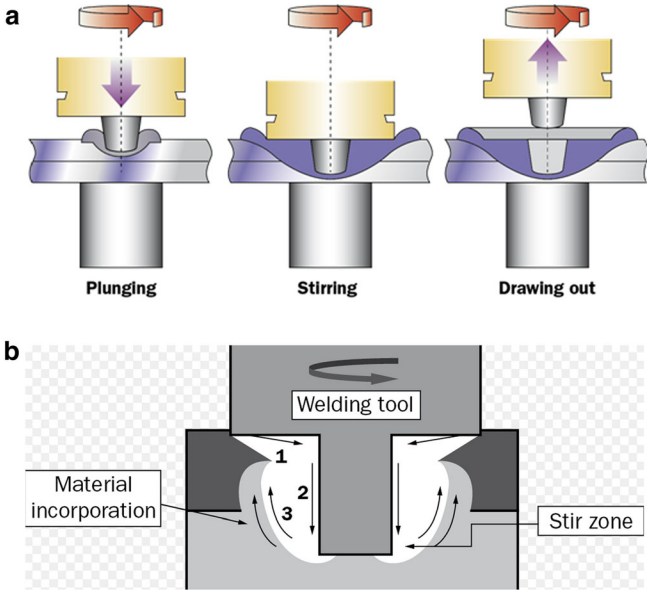

Fig. 9 **a** Friction stir spot welding phases [54]. **b** Material flow behavior during FSSW [55]

that the upper and lower sheet metal is incorporated at the pin root, before the stirred material moves towards the bottom, in particular when a threaded pin is used. A cylindrical, smooth pin without threading limits the continuous flow of material in vertical direction and the formation of a stirring region around the pin, as seen in Fig. 9b. The microstructure of the FSSW welded aluminum AA6061-T4 is given in Fig. 10.

Microstructure of FSSW has three distinct areas [56, 57]. These are stirring zone (SZ), thermo-mechanically altered zone (TMAZ), and thermally altered zone (HAZ), as shown in Fig. 10a. Increasing the rotation speed for the different plunging times corresponds to a resistance rise. When the plunging time is equal to 2 s, the percentage of resistance increase is quite small as the rotation speed grows. On the contrary, when the rotation is equal to 3 or 4 s, the growth rate is higher than that of 2 s. This study points out that improved welding properties can be attained with high rotation speed and long pause time. The welding microstructures can be subdivided into four regions, BM, HAZ, TMAZ, and SZ, and both a dynamic re-crystallization and dissolution of precipitates into the welding are highlighted, as seen in Fig. 10b. The tool geometries remarkably determine the final welding result, according to the process parameters [56]. The right matching between tool and process parameters determines the final result of the welding. Tensile shear test results of FSSW given in Fig. 11 indicate that the weld performance was significantly affected by the tool rotation, dwell time,

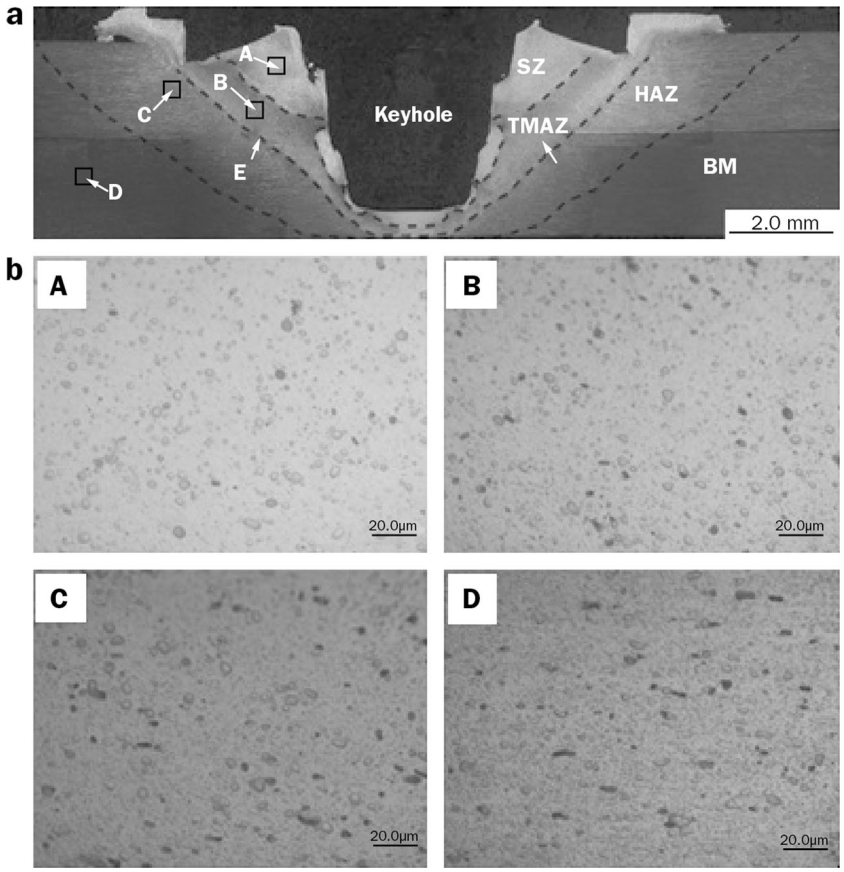

Fig. 10 **a** Microstructure of FSSW, **b** microstructure analysis for FSSW with 1200 rpm rotation speed and 4 s pause time [55], **c** overall macrograph of FSSW [55]

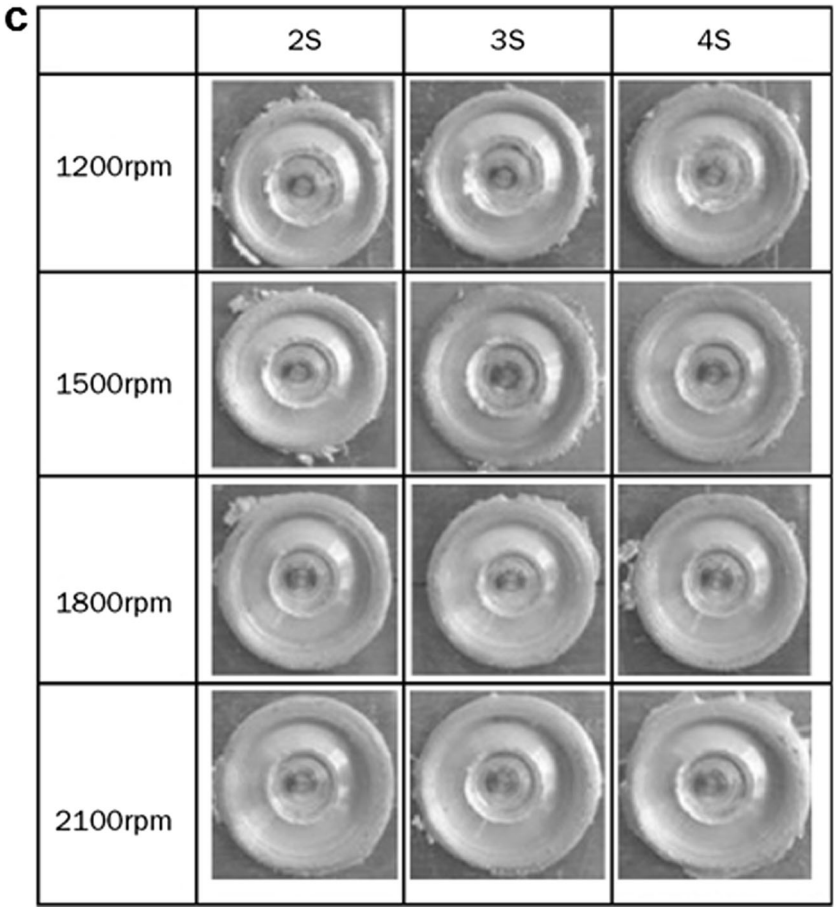

Fig. 10 (continued)

and the tool pin height [57]. The results of the tensile shear test indicate that there are optimum process parameters which give the highest tensile shear strength.

2.3 Refill friction stir spot welding process

One of the disadvantages of FSSW joint is that probe hole inevitably remaining at the center of the weld nugget reduces the joint strength and that corrosion could take place preferentially at the probe hole because rainwater remains in the hole, where body paint barely reaches the bottom [58–60]. There are very few publications about refilling of the probe hole during friction stir spot welding process [35, 61]. In order to avoid this situation, GKSS of Germany invented a process that would fill the key hole and this method was called the refill friction stir welding (RFSSW) process [59]. Stages of refill friction stir welding are given in Fig. 12. Top view and macroscopic appearance of a cross-section of the welds made by FSSW and RFSSW are given in Fig. 13. The figure shows that probe hole is successfully refilled by RFSSW. Venukumar

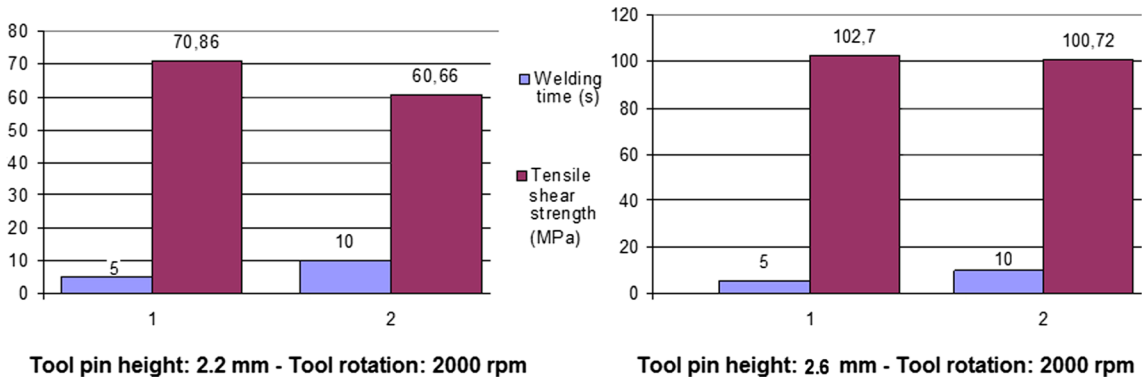

Fig. 11 Effects of welding parameters on the shear tensile strength of test samples joined with FSSW [57]

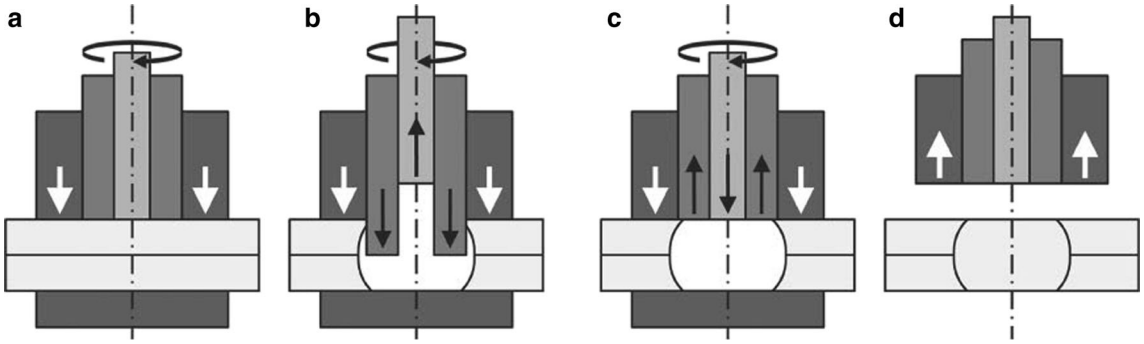

Fig. 12 Friction stir spot welding process variants: **a** clamping and tool rotation, **b** sleeve plunge and pin retraction, **c** tool retraction to surface level, **d** tool removal [60]

et al. [61] compared microstructure and mechanical properties of conventional FSSW and RFSSW for AA 6061-T6 sheets with 2 mm in thickness. The results of the study state that better static shear strength can be achieved at a rotational speed of 1800 r/min, while by conventional FSSW process better static shear strength was achieved at 900 r/min, as seen in Fig. 14. It can be observed from Fig. 14 that, by RFSSW, better static shear strength can be achieved. The improvement in static shear strength by RFSSW is found to be 38.5 % higher than that by conventional FSSW.

2.4 Cladding applications with friction stir welding

Cladding with friction stir welding allows deposition of thin clad layers on a substrate through a hollow tool, as seen in Fig. 15a. The developed process is entitled friction surface cladding (FSC), for a configuration without a central probe. The FSC technology enables the deposition of a solid-state coating using filler material on a substrate with good metallurgical bonding [62, 63]. A prototype of the modified friction stir welding tool is used. The weld properties strongly depend on the welding conditions. Important process parameters of FSC are the welding speed, the tool rotation rate, and the applied down force. Also, the type of tool and material grade play an important role. Material flow under the shoulder bottom of the rotating tool moving through the workpiece is required to improve the weld quality and speed of the welding process. Protective coating against wear and corrosion can be deposited, as seen in Fig. 15b.

2.5 Friction stir riveting

Friction stir riveting (FSR) is a new joining process for one-sided joining (compared with the two-sided access required, such as self-piercing riveting) of aluminum alloys, which eliminates the need to pre-drill a hole for rivet insertion. Stages of friction stir riveting are given in Fig. 16. A blind rivet rotating at high speed is brought into contact with the workpiece, thereby generating frictional heat between the rivet and the workpiece, which softens the workpiece material and enables the rivet to be driven into the workpieces under reduced force. Once fully inserted, the blind rivet is upset using

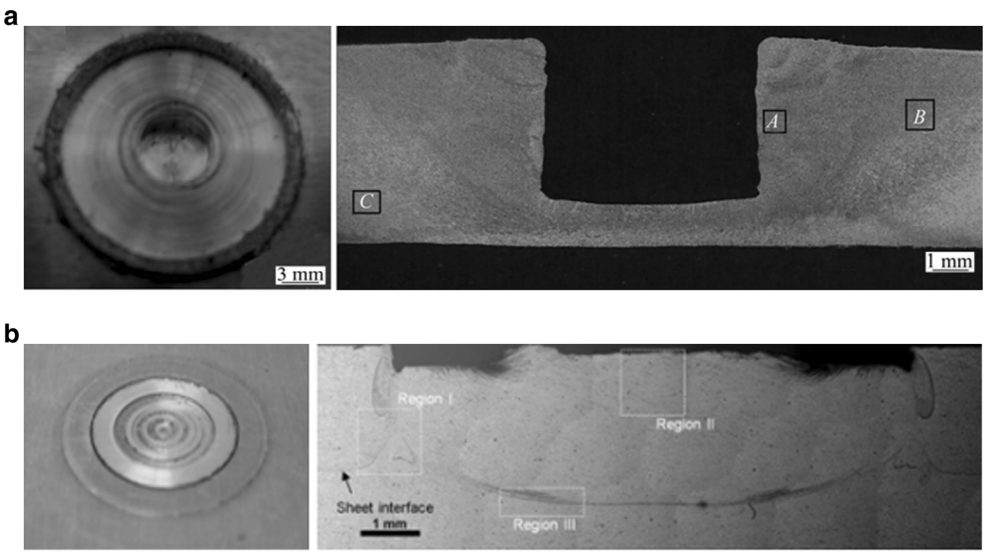

Fig. 13 **a** Top view and macroscopic appearance of a cross-section of the welds made by conventional friction stir welding-FSSW [61]; **b** refill friction stir welding-RFSSW [35]

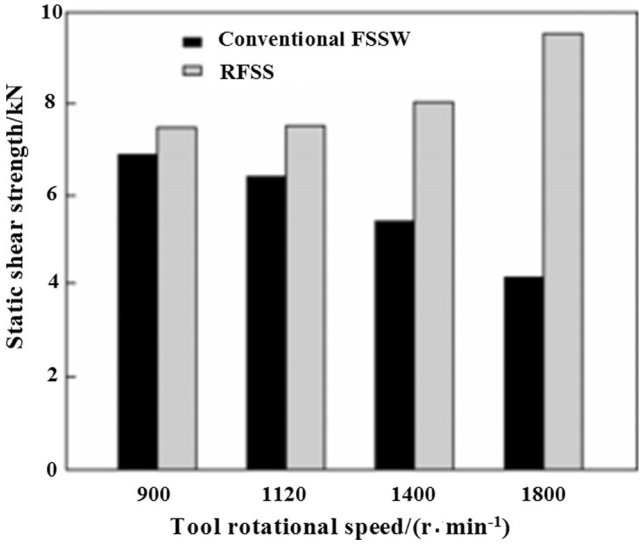

Fig. 14 Static shear strength of FSSW joints under different rotational speeds [61]

the internal mandrel (as in a conventional blind riveting process) to fasten the workpieces together. The quality of a riveted joint relies on the rivet, the mixed zone around rivet trunk, and the solid bonding between two sheets [63, 64]. Hence, the characterization of a joint produced by friction-stir riveting should be investigated from these three aspects. In the friction stir riveting process, the spindle speed, feed rate, feed depth, and the preheating time are the parameters that can be controlled. The rotation speed ranges from 500 to 3000 rpm, and the feed rate starts from 0.05 in. per min and rises by an increment of 0.05 in. per min [65]. The microscopic cross-section structure shows the mixed area in the vicinity of the rivet trunk where materials from different sheets becomes "one." This area is created by the rotating rivet which

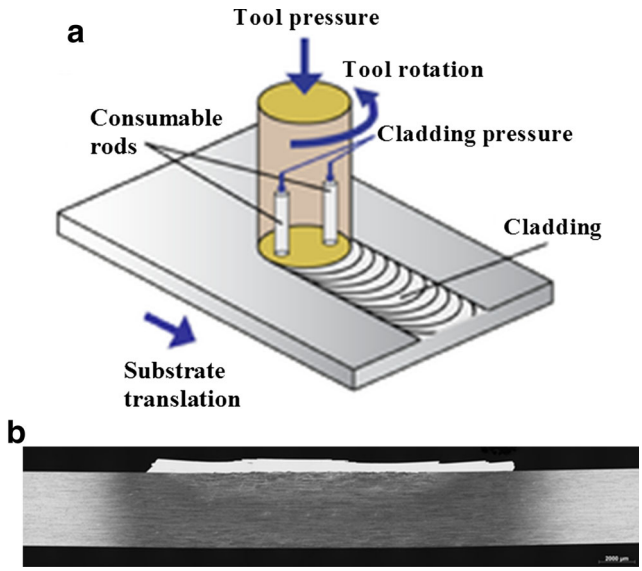

Fig. 15 Schematic representation of the friction surface cladding processes (FSC) [62]

stirs and mixes the sheet metals around it. This stirring motion generates heat and softens the sheet material around the rivet and finally "welds" these two sheets together. It is reasonable to assume that the behavior of the mixed zone performs akin to a piece of metal, if this zone is highly compacted by the riveting process. Consequently, the junction where the faying surfaces meet at the end of the interface determines the strength of the friction-stir rivet. The cross-sectional areas in the mixed zone are measured by the vertical distance to the end of the interface from the upper and lower edge inside the concave. These two distances are denoted as *dt* and *db*, respectively, as seen in Fig. 17. There is a gap between the cap of the rivet and the top of the mixed zone which is created by the riveting process [65]. This is created by two mechanisms. Insufficient filling of the space created by the advancing rivet head is the first mechanism. The cap part of the rivet has a larger dimension than the bottom. While the rotating rivets move into the aluminum, some amount of the material squeeze out. Another deficit is the volume shrinkage due to excessive heating. Such a gap reduces the cross-sectional areas of the top sheet near the rivet, as well as the restraint imposed by the rivet on the sheets. This situation reduces the strength of the joint. Friction stir blind riveting process can be carried out over a wide range of operating parameters. The robustness of the process against variations in operating conditions shows that the process can be carried out without high-end equipment and without requiring precise initial setup. It also suggests that the process is feasible for rapid joint fabrication in volume production [66–68]. Better static and fatigue strength from the friction stir blind riveting process are obtained when compared with conventional spot welding.

3 Friction stir processing

Friction stir processing (FSP) is a new technology and a kind of FSW that can be used to enhance or modify material properties [3]. FSP has been demonstrated to be capable of removing local defects and locally modifying material properties, such as ductility, fatigue life, and fracture toughness. FSP is used to transform a heterogeneous microstructure to a more homogeneous, refined microstructure [3, 47]. There are several possible methods available which can be applied to a variety of material shapes and sizes. In many cases, the reprocessed areas have superior strength and formability than the parent material, e.g., aluminum castings can be processed to consolidate voids [9, 47–49]. The strong demand for weight reduction in car and marine fabrications urges the optimization of the design of products employing low weight materials [48, 49]. For many applications, the useful life of components often depends on their surface properties such as wear resistance. FSP can be used to improve surface properties of metallic materials. On observing the advantages associated with

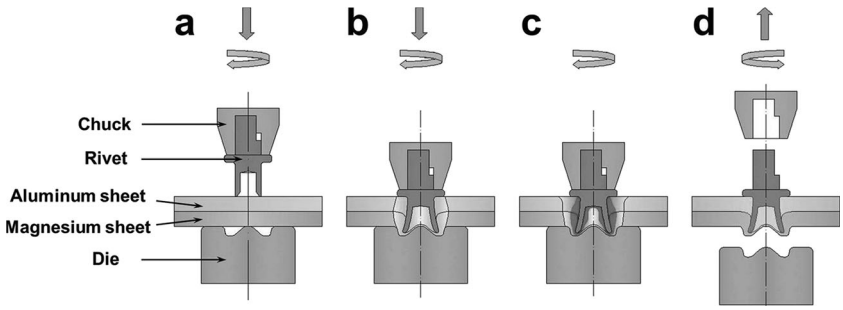

Fig. 16 Friction stir riveting variants: **a** clamping and tool rotation, **b** rivet plunge, **c** fixturing, **d** tool removal [64]

FSW, mainly grain refinement, the phenomenon has been extended to processing commercial alloys [12, 21]. There are several friction stir processing techniques that can be used in industrial applications. These processes are given below.

3.1 Grain refinement by FSP

FSP improves ductility, formability, and mechanical strength on account of homogenized microstructure with equiaxed fine grains [22]. FSP uses the same methodology as FSW; however, it utilizes this to modify the local microstructure. A schematic illustration of FSP is shown in Fig. 18. FSP has proven to be successful in the modification of various properties such as formability, hardness, yield strength, fatigue, and corrosion resistance [13, 22]. The rubbing of the rotating shoulder generates heat, which softens the material (below the melting temperature of the sheet), and with the mechanical stirring caused by the pin, the material within the processed zone undergoes intense plastic deformation, yielding a dynamically recrystallized fine grain structure [69]. Several investigations have been done about the effect of FSP on various properties of metals, especially on Al and Mg alloys. Elangovan and Balasubramanian studied the effect of tool profile and rotation speed on AA 2219 and AA 6061 [14, 69]. Hsu et al. [70] achieved ultrafine grained Al–Al2Cu composite by FSP, which has high Young's modulus, good compressive strength, and reasonably good compressive ductility. Santella et al. [71] studied the effect of FSP on the mechanical properties of cast A356 and A319 Al alloys and observed that the cast dendritic structure was replaced with a fine equiaxed structure in the stir zone and the tensile strength, ductility, and fatigue life of both alloys improved by FSP. Surekha et al. [72] studied the effect of multipass FSP on the corrosion behavior of AA 2219 and found that corrosion resistance of aluminum alloy increased with increase in number of passes.

Behnagh et al. [48] investigated the variation of friction coefficient with sliding distance for 5083 aluminum rolled plate base material (BM) and friction-stirred (FS) processed samples. Friction coefficients are presented in Fig. 19. The average friction coefficient of the BM (Fig. 19a) was found to be 0.62, as indicated by high fluctuations in the friction curves. The average friction coefficient of the friction stir processed sample oscillates around approximately 0.33, which is obviously much lower than that of BM (Fig. 19b). The relationship between weight loss and the sliding distance of BM and FS processed samples is given in Fig. 20a. As seen in Fig. 20 for both BM and FS processed sample, the wear weight loss increased with sliding distance; also FSP was found to be beneficial in improving wear resistance under applied load of 10 N. The high wear resistance of the stirred zone is attributed to a lower coefficient of friction. Figure 20b shows the wear rate (weight loss divided by the sliding distance). The BM wore much more rapidly than the FS processed sample. Close comparison of Fig. 20a, b also reveals that the amount of wear weight loss and the wear rate of the samples are significantly lower in the FS processed samples compared to the BM. Hardness variations of FS processed and as-cast samples are given in Fig. 21. Hardness test reveals that

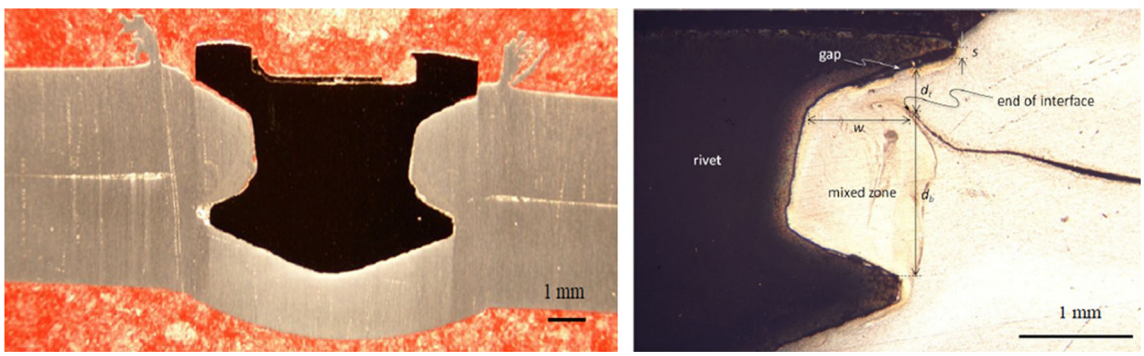

Fig. 17 Metallographic sections of a friction-stir riveted joint dimensions and various zones for characterizing the joint [65]

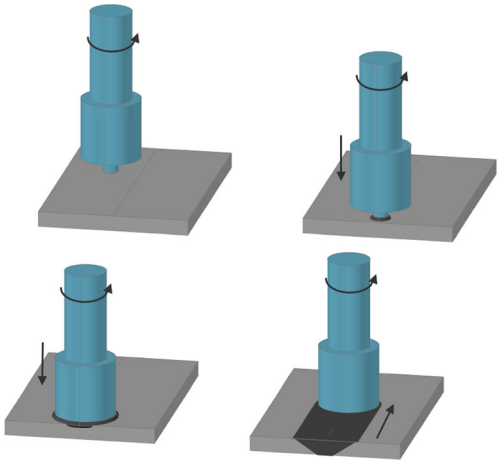

Fig. 18 Schematic representation of the FSP principle [51]

the FS processed A356 displays higher hardness compared with the as-cast A356 [73]. This is attributed to remarkable microstructural refinement, homogenization, and densification [74–76]. Figure 21 also reveals that the incorporation of SiCp into the surface layer of A356 Al alloy via FSP significantly increases the hardness of Al substrate. Shinoda and Kawai [76] studied the modification in the solidification microstructure of friction stir-welded Al alloy castings. According to their observations, hardness, increased in the stir zone due to the modification, breaking up and homogenization of the Si needles in the eutectic phase. Uniform dispersion of the SiCp, which has an extremely high hardness, and significant microstructural modification due to FSP results in an increase in the hardness [77].

3.2 Surface modification of porous metals using friction stir process

Kwon et al. [78] modified the surface region of the aluminum foams (trade name ALPORAS) with FSP using friction phenomena with a high-speed rotating tool, as seen in Fig. 22a. The tool was rotated at speeds ranging from 820 to 2400 rpm and plunged from the top surface of the aluminum to a depth of 2.6 mm from the top surface of the aluminum foam and then traversed at speeds ranging from 50 to 300 mm/min. The

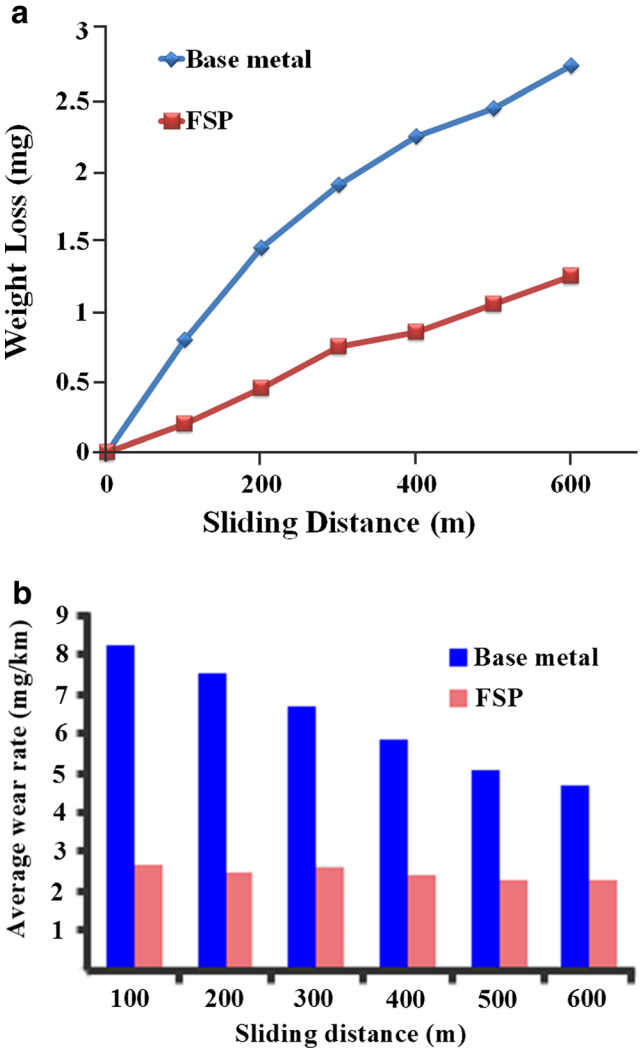

Fig. 20 **a** Relationship between weight loss and the sliding distance [51] and **b** comparison of wear rate of base material and FS processed sample [51]

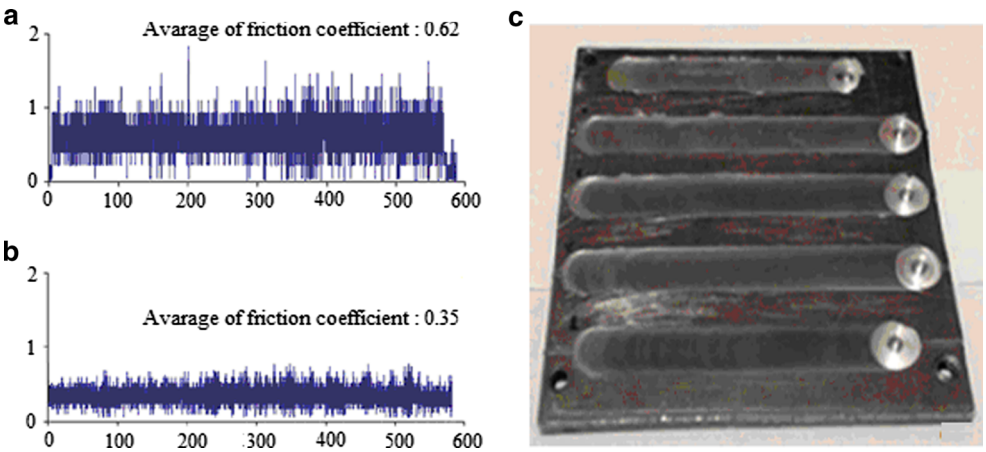

Fig. 19 Variation of friction coefficient with sliding distance, **a** base material and **b** FS processed sample, and **c** FSP sample surface (1400 rpm and 63 mm=min) [51]

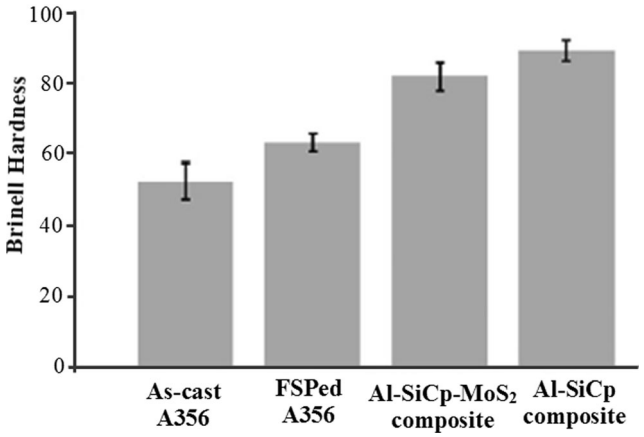

Fig. 21 Variation of Brinell hardness in as-cast, FS processed A356, and composite samples [58]

surface modified zone and the unprocessed zone are labeled SMZ and UZ, respectively. *X*, *Z*, and *Y* represent the tool traverse direction, the tool rotation axis direction, and the width direction of porous metal, respectively. SMZ had considerably smoother surface in comparison to the UZ. Especially for 1390 rpm and 150 mm/min, the smoothest surface was obtained, which was attributed to the smaller amount of pores in the SMZ. In addition, a very dense layer was formed near the surface of the SMZ through the localized collapse and densification of the cell structure near the surface region, which was attributed to the friction phenomena with the high-speed rotating tool. The mechanical properties of the aluminum foams were significantly improved through the FSP. Especially for 1390 rpm and 150 mm/min, the SMZ exhibited the highest average maximum indentation strength and energy absorption ability, which were equivalent to about 2.2 times the values of the UZ due to the reduction of pores after SMZ. The tool rotation speed and the tool traverse speed are important parameters not only in controlling the surface morphology, but also in improving the mechanical properties of the aluminum foams. The FSP was a very effective technology for the remarkable improvement in the mechanical properties through the cell structure control of the surface region of the aluminum foams, without any dense skin materials. In the recent past, there has been a remarkable increase in research on porous metals with extremely low relative densities which are attributed to their cellular structure with a great number of pores [79–83]. Figure 22b shows a typical optical macrograph of the cross-sections perpendicular to the tool traverse direction (*X*-axis direction) of the FS processed aluminum foams [78]. The surface region of the UZ is composed of the open pores, although the closed pores were observed in the inner region. In contrast, a very dense layer was formed near the surface of the SMZ. Cell wall material had been plastically deformed near the surface region by the high speed rotating tool during the FSP. The buckling of the cell wall was observed beneath the dense surface layer of the SMZ. SMZ

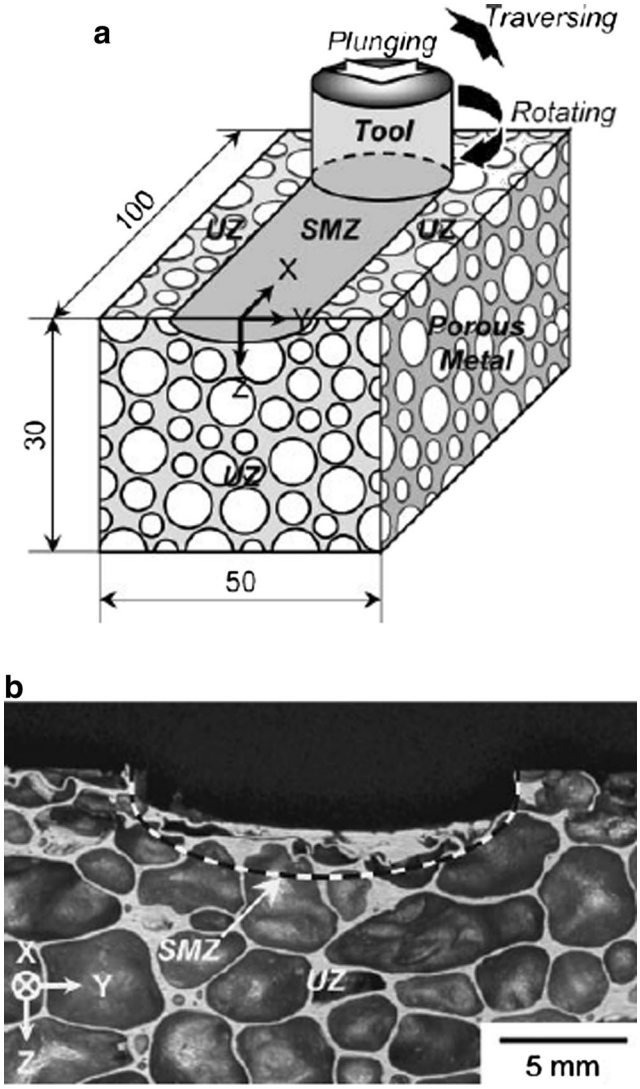

Fig. 22 **a** Schematic illustration showing the basic principle of the friction stir processing of porous material. **b** Typical optical macrograph of the cross-sections perpendicular to the tool traverse direction of the surface-modified aluminum foam [78]

had been formed by the localized collapse and densification of the cell structure near the surface region, which was attributed to friction phenomena with the rotating tool. In addition, these results demonstrate that the FSP is a very effective technology in forming the dense layer near the surface of the porous metals.

3.3 Friction stir channeling

Recently, friction stir channeling (FSCn) was patented and reinvented by Vilaça and Vidal [84]. An evolution of the FSCn tool was developed, which enables the material removed by the process to be cleared out as the channel is being produced by leaving the workpiece with the same level and surface finish as it had before the channel was produced. The major step given by Vilaça and Vidal for FSCn reinforces the great

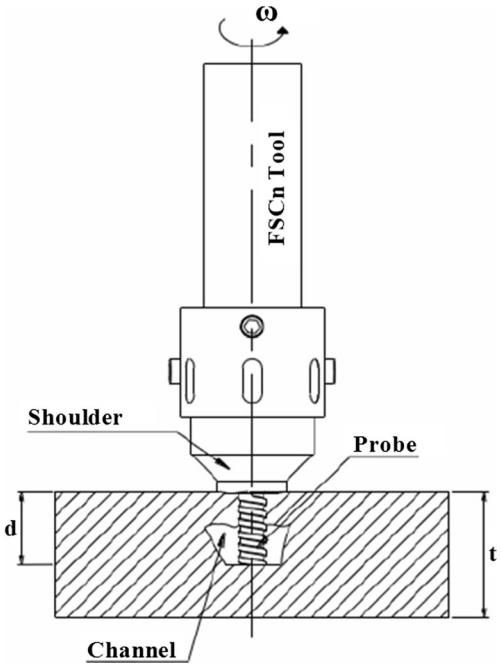

Fig. 23 Schematic representation of FSCn "new version" process (cross-section view) [87]

potential of this manufacturing process in industrial applications such as the automotive, aerospace and railway industry, as well as conformal cooling systems and heat exchangers, as it was mentioned by Balasubramanian et al. [85]. FSCn has two main areas of interest in the world industry: *Molds and Heat Exchangers*. Balasubramanian et al. [86] stated that the presence of the gap between the shoulder and the workpiece was a major difference between the FSCn and the normal FSW or FSP. It is important to recognize that FSW and FSP are performed with the bottom of the shoulder in contact with the workpiece in order to generate the forging action required to produce defect free welding or processing as seen in Fig. 23. However, the "new version" of FSCn produced by P. Vilaça et al. [84] suggests some modifications from FSCn initial version of Balasubramanian. No initial clearance is provided between the shoulder and the workpiece, so the material from the base of the probe is deposited on the sides and back of the shoulder (to create the channel). The main parameters of the process (tool travel speed, tool rotation speed, the size of the probe, and shoulder) can be adjusted to control the shape, size, and integrity of the channel. Vilaça and Vidal [84] controlled the amount of material that flows from the processed zone to produce the internal channel. It is also possible to integrate in the tool, a surface finishing feature. The friction stir (FS) channels result from the application, in the visco-plasticized workpiece material, of an upward action along the threaded probe combined with an outward action along the scrolled shoulder. The FSCn process can be controlled by selecting the adequate processing parameters.

The material that comes from the base of the probe is pushed outwards by the scrolls on the shoulder because there is no clearance between shoulder and workpiece. This major difference also has an impact on the characteristics of the channel: size, shape, roughness, and mechanical properties, compared to the FS channels produced by Balasubramanian. The development made by Vilaça et al. [84] created this "new version," which allows FSCn to have channels of greater dimension, rougher surfaces and bigger "wet surfaces." Consequently, all of the features enable more industrial applications for FSCn. The differences in the FSCn process between the two versions also caused a consequent difference in the channel shapes. The shape of the channel obtained from FSCn initial version is closer to an ellipse or oval shape. The author stated that the channel shapes usually vary nonlinearly with the process parameters (the tool rotation speed and tool travel speed). Figure 24 shows the variation of the channel shape by changing the process parameters in the FSCn initial version. As it can be observed in Fig. 24, including (a) and (b), the channel produced with a high heat index (Fig. 24a) process condition is visibly well-structured as compared with the channel from the lower heat index (Fig. 24b) process condition. In this case, Balasubramanian [86] defined heat index as a relative term defined as the ratio of the square of the tool rotational speed to the tool travel speed. This ratio is used as a representation to differentiate the various processing conditions. For a high heat index run, the volume of material displaced from the probe base is high due to the high tool rotation speed, or alternatively, a low travel speed. Another aspect that can be easily spotted in the channel shape is the shape of the channel side walls, which are clearly influenced by the probe features.

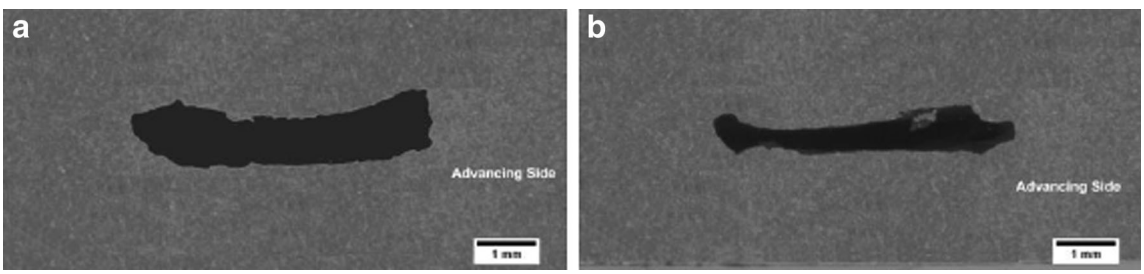

Fig. 24 Cross-section showing FS channel shapes produced by with different processing parameters: **a** 1100 rpm, 2.11 mm/s and **b** 1100 rpm, 2.96 mm/s [86]

The channel shape in the "new version" FSCn is given in Fig. 25a. Geometric parameters of the FS channel cross-section are demonstrated in Fig. 25b. The form of the channel can be attributed to the volume of processed material that is displaced from the base of the probe during each rotation of the tool and also the compacting force that is applied on the channel ceiling during the linear forward movement performed by the shoulder [87]. Nonetheless, a trend can be spotted in the four different conditions of the "new version" FSCn. Condition B has by far the smallest heat index, and it has the channel with the least defined shape. On the other hand, conditions A and D have very similar heat indexes, but the channel ceiling of condition D demonstrates a very irregular surface which may be due to a very large amount of frictional heat produced and an excessive softening of the workpiece material. A possible cause of this situation can be the elevated value of tool rotation speed. However, it is clear that the channel shape has small variations compared to the considerable modification of the process parameters values. In order to standardize the characteristics of the channel shape with the variation of the process parameters, two characteristics of the channel were determined by Vidal et al. [87]: the closing layer thickness (D) and the shear angle (α). Figure 26 shows the final injection mold prototype produced by FS channels, including a compact, solid cavity mold at the left, and a sectioned mold cavity at the right. The development of a technology is always subject to the necessity of the industry. The potential, or value, of a technology is related to the amount of solutions it can provide to the industry. The industry is always searching for a better solution or an easier way to solve problems. Consequently, if a new technology is being developed, it is of major importance to analyze its possible industrial applications. In this case, FSCn has two main areas of interest in the world industry: *Molds and Heat Exchangers* [88–90]. Two ways of producing molds, which FSCn can be an alternative to are: *Conformal Cooling* and *Rapid Prototyping*.

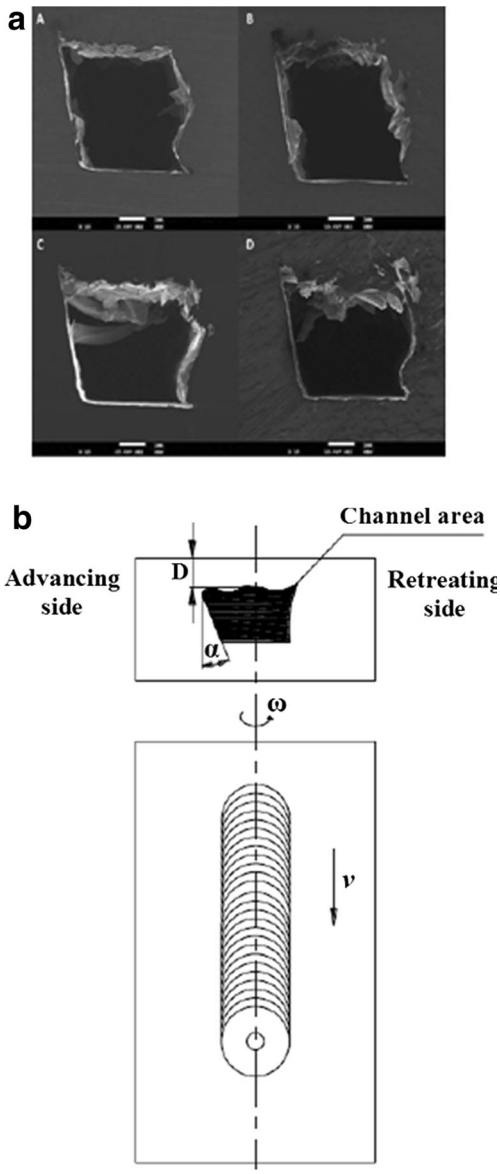

Fig. 25 **a** Cross-section macrograph showing channel geometries produced with different FSCn processing parameters: (*A*) 600 rpm, 80 mm/min, (*B*) 600 rpm, 150 mm/min, (*C*) 800 rpm, 80 mm/min, and (*D*) 800 rpm, 150 mm/min. **b** Schematic representation of a cross-section (*above*) and a plan (*below*) views of the friction stir channeled solid block [88]

3.4 Surface hardening by friction stir processing

Fujii et al. [91] used the FSP for surface hardening of cast irons. In this study, friction stir processing (FSP), whose principle is the same as friction stir welding, was used as one of the surface treatment methods for cast irons. Flake graphite cast iron (FC300) and nodular graphite cast iron (FCD700) were used to investigate the validity of this method. They used a rotary tool with a 25-mm diameter cylinder. Traveling speed was varied between 50 and 150 mm/min in order to control the heat input at the constant rotation speed of 900 rpm. As a result, it has been clarified that a Vickers hardness of about 700HV is obtained for both cast irons. They reported that when a tool without a probe is used, the domain in which graphite is crushed and striated is minimized. This leads to obtaining a much harder sample due to the formation of a very fine martensite structure. This structure is created by the heating the surface very locally and then cooling by a very high rate [40, 92]. The hardness change depends on the size of the martensite, which can be controlled by the process conditions, such as the tool traveling speed and the load. Based on these results, it was clarified that the FSP has many advantages for cast irons, such as a higher hardness and lower distortion. As a result, no post-surface heat treatment and no post-machining are necessary to obtain the requisite hardness, while these processes are generally required when using the traditional methods [91]. For ferroalloys, on the other hand,

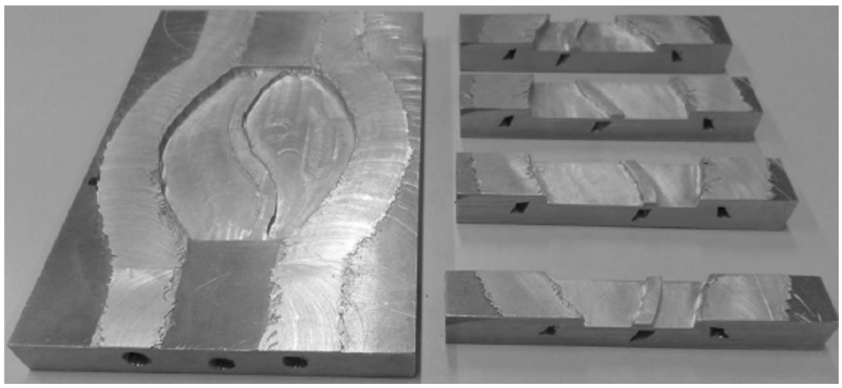

Fig. 26 Injection mold prototype produced by FS channels, including at the left a compact, solid cavity mold and at the right a sectioned mold [88]

there is no report concerning the FSP because issues, such as the durability of the tool, have to be solved, although some research studies on friction stir welding have begun [40, 92, 93]. Five-mm-thick flake graphite cast iron (FC300) and nodular graphite cast iron (FCD700) plates were surface hardened by FSP. The modified region becomes narrower when compared to the 50 mm/min case. The formation of the defects is significantly related to the heat input. When the heat input is insufficient, for example, under the conditions of 900 rpm and 2×10^3 kgf, a defect is formed during the early stage by scooping out the material, as shown in Fig. 27.

When the heat input is excessive, the surface material is peeled off as if the material is melted because it softens too much. A good microstructure formed by the plastic flows without the surface being peeled off can be obtained by controlling the heat input properly. Therefore, it is necessary to adjust the process conditions, such as the rotation speed and the traveling speed, in order to optimize the heat input. Figure 28a shows the Vickers hardness distribution in the depth direction on the central part and at 6 mm from the center on the advancing side and the retreating side on a cross-section vertical to the welding direction after the FSP. It was found that a high and comparatively steady hardness is obtained in the area from 0.2 to 1.0 mm in depth while a low value was observed at 0.1 mm from the surface. The hardness between 0.2 and 1.0 mm exceeds 700 HV.

Figure 28b shows the microstructure of nodular graphite cast iron at a high magnification. A very fine needle-like martensite structure is observed. It is considered that this structure was generated because the material was locally heated and rapidly cooled during the FSP. On the other hand, the size and density of the martensite are changed even in the same martensite structure. Figure 29a shows the Vickers hardness distribution of the flake graphite cast iron friction stir processed in a way similar to the nodular graphite cast iron. An average value higher than 700 HV is obtained to about 1 mm depth and values higher than 800 HV were also measured at many points. Figure 29b shows the microstructure of flake graphite cast iron. A martensitic structure is formed throughout the region. It can be seen in Fig. 29a that the hardness of the central part decreases near the surface. Since the hardness of the base material is lower, the bottom of the tool enters more deeply compared to the FCD 700. Accordingly, the domain is expanded, where the graphite was crushed and striated by plastic flow, and the hardness decreased [91].

4 Additive friction stir processing

Additive manufacturing (AM) techniques such as weld overlay and laser engineered net shaping (LENS) can be used in conjunction with friction stir processing (FSP) [63, 94].

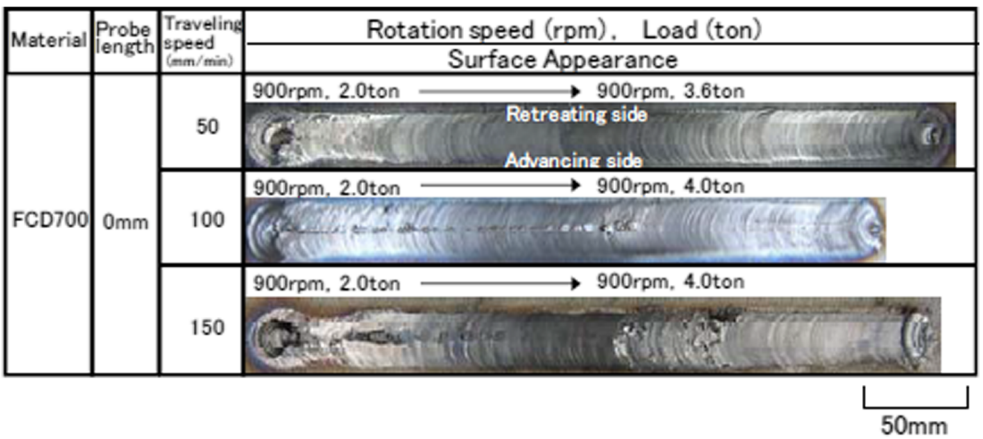

Fig. 27 Appearance of FS processed FCD700 cast iron [91]

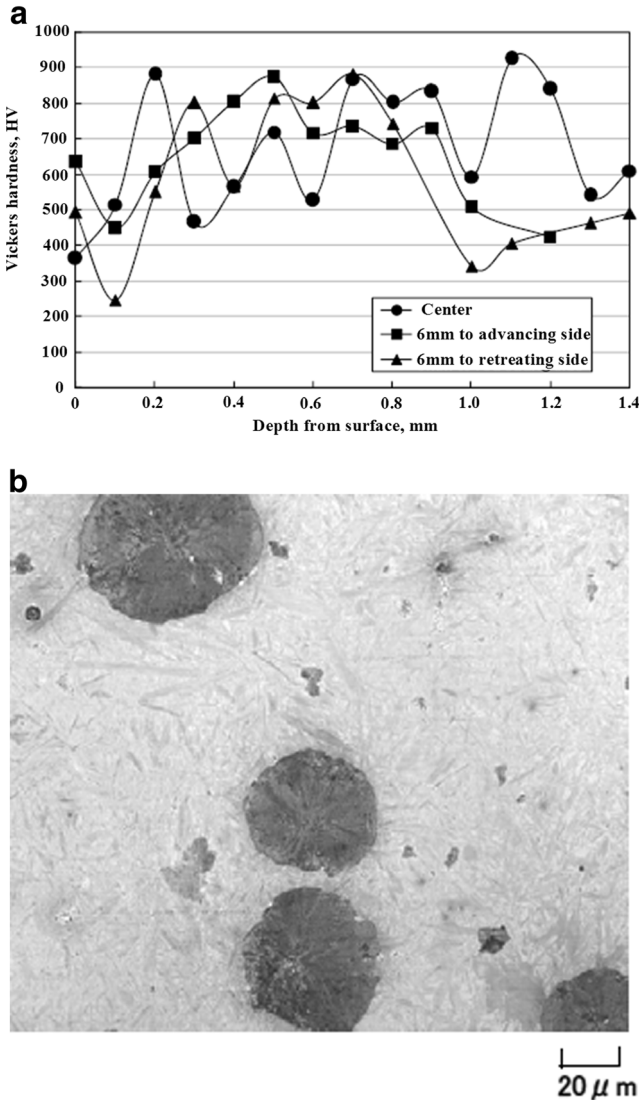

Fig. 28 **a** Vickers hardness distribution of FS processed nodular graphite cast iron. **b** Microstructures of FS processed nodular graphite cast iron FCD700 [91]

Additive manufacturing techniques, while providing many advantages with respect to near net shape manufacture, are often susceptible to high defect rates, including porosity, lack-of-fusion, cold laps, etc. [94]. The use of FSP in conjunction with AM processes offers the possibility of reducing defects density, eliminating segregation, and providing grain refinement. Friction stir processing is typically an autogenous process requiring no filler/additive material. However, by incorporating additive methods, local chemical composition and/or phase content can be combined with the beneficial microstructural modification of the friction stir process. Severe plastic deformation under forging pressure of the friction stir tool also has the ability to improve the as-deposited microstructure of the original additive process via grain refinement in addition to the elimination/reduction of discontinuities from the additive process [63, 94]. One possible schematic illustration of the additive friction stir processing (AFSP) process is shown in Fig. 30. The generic AFSP depicted in the illustration incorporates an additive process. This additive process could include fusion base additive processes such as laser-engineered near net shaping (LENS), thermal spray, laser-assisted direct metal deposition, etc. Solid-state additive processes such as cold spray, kinetic metallization, or selective laser sintering (SLS) could also be utilized as additive techniques [35, 62, 63, 94]. Because the microstructure will be changed drastically, the additive process utilized, parameters, and even deposition quality are not of great importance as long as the additive material can adhere to the substrate [95–97]. It can be postulated that AFSP can enable the use of high deposition rates of additive material because any cracks or discontinuities formed during deposition will be eliminated, thus increasing overall productivity. FSP can be used to both modify the starting microstructure and to improve the properties of material added via an AM process [98–100].

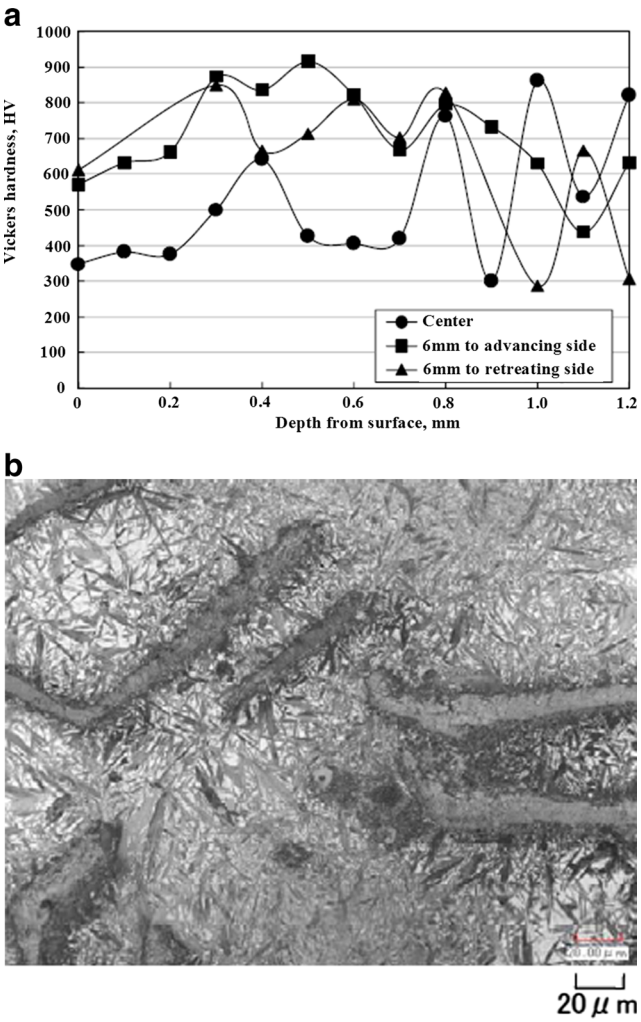

Fig. 29 **a** Vickers hardness distribution of FS processed flake graphite cast iron. **b** Microstructure of FS processed FC300 [91]

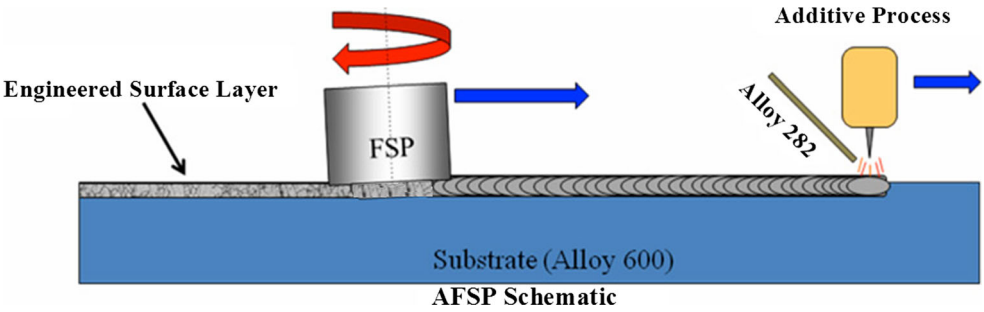

Fig. 30 Additive friction stir processing [88]

Considerable improvement in properties can be achieved by such hybrid processing [101–103]. For example, MarM-247 (a high volume fraction gamma-prime Ni base alloy) can be deposited using the LENS process and then FS processed to produce very high hardness, surface layers on Alloy 600 in the as-processed condition, as shown in Fig. 30. Alloy 600 (UNS designation N0660) is a nickel–chromium non-magnetic alloy designed for use in applications that require corrosion and high temperature resistance. Such benefits in surface engineering were also demonstrated with "Haynes 282" nickel-based superalloy with good high temperature mechanical properties [94].

5 Composite manufacturing processes by friction stir process

The solid-state nature of FSP is advantageous for Al- and Mg-MMC fabrication because very limited or no reactivity occurs between the matrix and reinforcing phase during processing [95]. Other higher temperature processing routes involving liquid phases lead to deleterious reactions between the matrix and the reinforcing phase. In its current state, the solid-state nature of FSP makes it an attractive method for site-specific fabrication of near-surface light metal-based MMCs. Mishra et al. [95] added WC to AA7050, single-wall carbon nanotubes to AA7075 [96] and SiC to AA5083 [97] via FSP. In a study by Fujii et al. [98], copper powder was incorporated via FSP in commercially pure AA1050 by filling an intentional gap between two Al plates in a butt configuration with Cu powder. Macroscopically, the distribution of Cu particles in the Al matrix was not uniform even after FSP by two overlapping passes, as seen in Fig. 31. However, micro-hardness measurements of the double pass runs show the SZ exhibits micro-hardness nearly twice the base metal hardness of 45 HVN. Upon further examination of these regions using TEM, the presence of nano-scale Al_2Cu precipitates was observed. These precipitates led to the increased hardness within the SZ [98]. High temperature AFSP was reported by Shamsipur et al. [99]. In this work, AFSP was used to create location-specific Ti/SiC composites. SiC powder was introduced into the Ti plate via powder-filled channels. Up to four overlapping passes were used to create a homogenous distribution of nano-sized SiC particles within the SZ, as seen in Fig. 32. The microhardness values of composites approximately 3.3 times greater than the as-received CP Ti-alloy had been fabricated. The authors observe the presence of nano-size SiC within the SZ that contribute to the high hardness in two ways. The high intrinsic hardness of SiC particles within a composite microstructure increased hardness. Secondly, the nano-scale SiC particles contributed significantly to grain boundary pinning. The restriction of grain boundary mobility during dynamic recovery/recrystallization led to the development of a highly refined stir zone microstructure with an average grain size of 400 nm. Under identical FSP parameters without the addition of SiC particles, the average grain size was an order of magnitude larger. The authors believed a reaction of the Ti matrix, and reinforcing SiC particles occurred as a result of AFSP; however, this was not directly observed. Additive FS processes involving dissimilar materials or additions of materials to react with the parent matrix upon processing for high melting point systems is limited. Incorporation of additional materials or dissimilar high melting point alloys by AFSP to locally enhance material properties/performance is a promising subject that warrants further study.

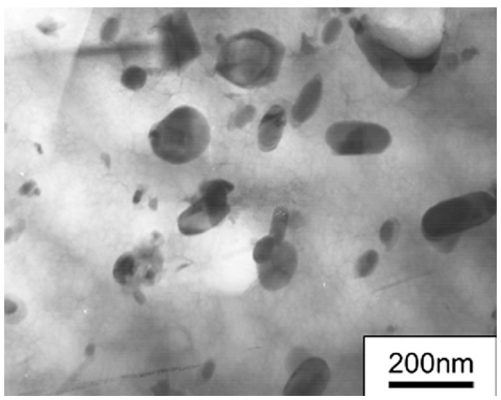

Fig. 31 Bright field TEM micrograph of Al2Cu precipitate formation after two FSP passes [98]

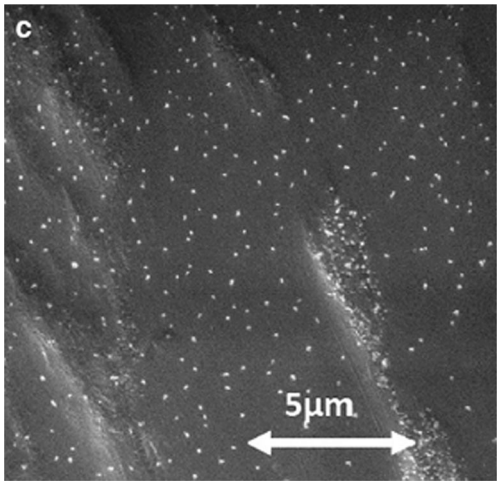

Fig. 32 Electron micrograph of SZ after four passes in AFSP CP-Ti+ SiC. Bright particles correspond to SiC clusters [99]

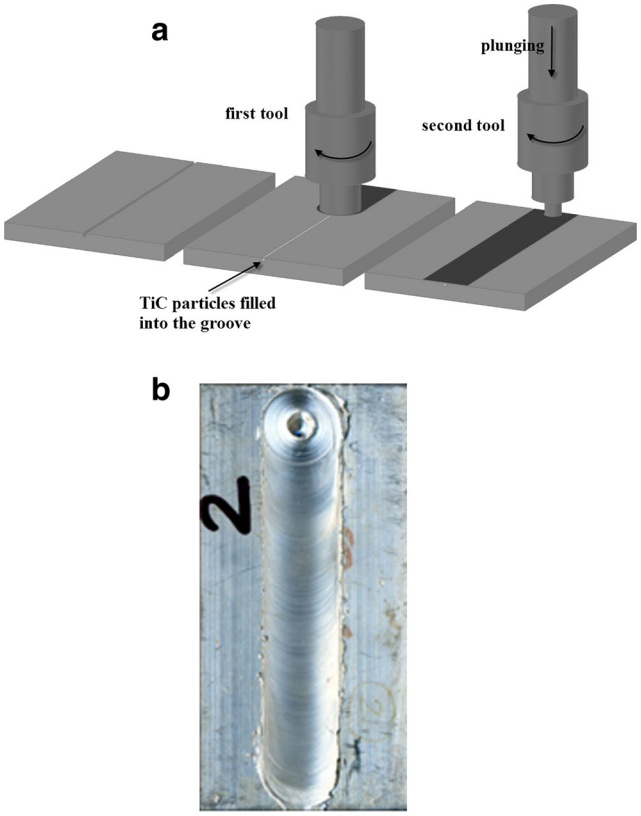

Fig. 33 **a** Schematic illustration of FSP steps. **b** Crown appearance of the FSP zone of AA1050/TiC surface metal matrix composite (SMMCZ) [103]

5.1 Fabrication of surface composite using friction stir processing

Thangarasu et al. [103] fabricated surface composite on the surface of pure (98.2 %) 1050 aluminum using friction stir processing. A grove of 0.5 mm in width, 5.8 mm in depth, and 100 mm in length was made on the plate and filled with TiC powder (≅2 μm). A FSP tool made of HCHCr steel, oil hardened to 62 HRC, having a cylindrical profile had been used, as seen in Fig. 33a. The tool had a shoulder diameter of 18 mm, pin diameter of 6 mm, and pin length of 5.8 mm. The FSP had been carried out at a rotational speed of 1600 rpm and a traverse speed of 60 mm/min. A downward force of 10 kN had been applied to the tool. FSP procedure is schematically shown in Fig. 33a. A tool without probe had initially been employed to cover the top of the grooves after filling with TiC particles to prevent the particles from scattering during FSP.

Figure 33b shows the upper surface appearance of the fabricated SMMC. The groove is effectively closed subsequent to FSP. The top surface shows very smooth quality, and there are almost no prominences or depressions in spite of the tool's stirring. Figure 34a shows the macrograph of the FSP zone. A defect-free FSP zone is observed. It is evident from the macrograph that the groove is completely bonded to all sides. The pin length is 0.3 mm higher than that of the groove depth which proves to be adequate to produce full penetration. Hence, defects do not arise at the bottom side of the groove [63]. The vigorous stirring action of the tool distributes the packed TiC particles into the plasticized alloy. The translation of the tool moves the plasticized composite from advancing side to retreading side and forges at the back of the tool. Thus, SMMC is produced by FSP. The FSP zone is typically about the size of the rotating pin, namely width and depth of 6 and 5.8 mm, respectively. Figure 34b shows the SEM micrographs of the interface zone at the retreading side between surface composite and aluminum alloy substrate. The surface composite layer appears to be well-bonded to the aluminum alloy substrate, and no defects are visible at the interface. A narrow thermo-mechanically affected zone (TMAZ) is observed. TMAZ exhibits the distribution of TiC particles along parallel bands in the aluminum matrix. Figure 35 shows the SEM micrographs of FSP zone. TiC particles are homogeneously distributed in the FSP zone. The grain size of the aluminum alloy has obviously been refined by FSP. A homogenous distribution of ceramic particles is essential to attain higher mechanical properties in SMMC. Stirring causes higher plastic strain which results in rearrangement of TiC particles. Disintegration of ceramic particles was widely acknowledged in FSW of aluminum matrix composites [100–102]. Investigators reported the blunting of sharp edges of Al_2O_3 or SiC particles (>20 μm) resulted in the formation of fine debris in the weld zone [100–102]. The difference in the size of particles in the SMMC, as seen in Fig. 35, is the least which indicates little or no disintegration during FSP [103]. This can be attributed to the initial morphology and size of TiC particles. TiC particles had a minimum number of sharp edges and less than 5 μm in size, which resulted in little or no disintegration. Figure 36 shows the micro-hardness distribution in the base alloy and composite. TiC particles enhanced the

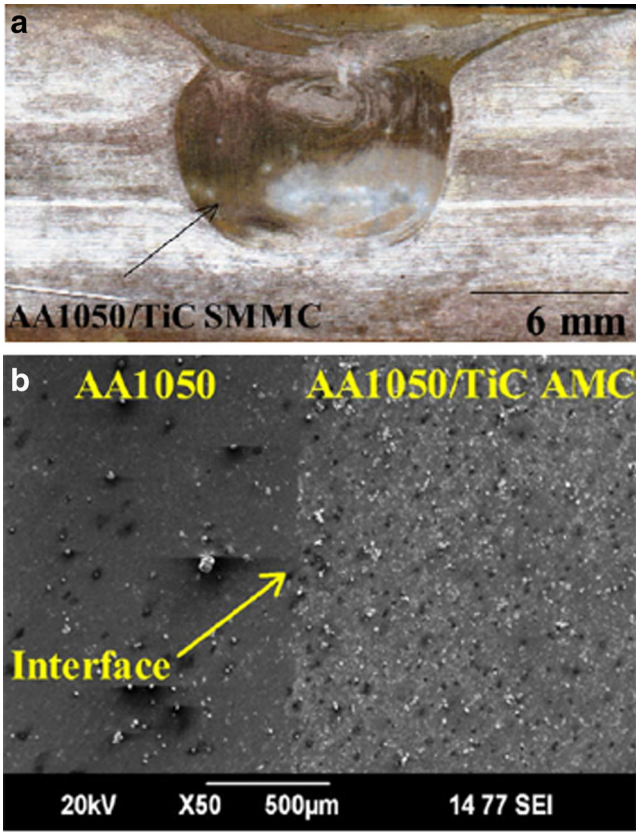

Fig. 34 **a** Macrograph of FSP zone. **b** SEM photomicrograph of interface zone [103]

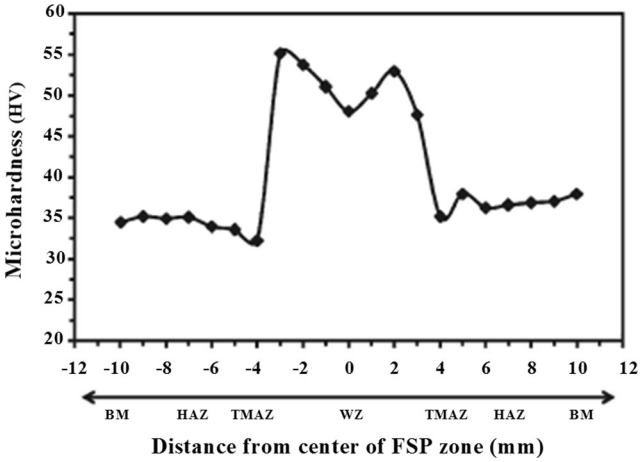

Fig. 36 Micro-hardness distribution in the base metal and composite [93]

hardness of aluminum alloy. The average hardness of FSP zone is 45 % higher than that of the aluminum alloy. The possible strengthening mechanisms which may operate in SMMC are as follows: Orowan strengthening, grain and substructure strengthening, quench hardening resulting from the dislocations generated to accommodate the differential thermal contraction between the reinforcing particles and the matrix, and work hardening due to the strain misfit between the elastic reinforcing particles and the plastic matrix [2, 3, 23]. The peak hardness is observed away from the center at the advancing and retreating sides. The material flows in a complex fashion from the retreating to the advancing side during FSP giving rise to gradients in temperature, strain, and strain rate across the stir zone. This in turn gives rise to different micro-structural features at different locations in the stir zone. Moreover, since a groove was made at the center of the aluminum plate to incorporate the TiC particles, the material has to flow into the groove to fill it to give a defect-free continuous stir zone. Hence, friction stir welding and processing both take place at the center while only friction stir processing takes place away from the center. Therefore, the center may experience less deformation compared to the sides. This may also be responsible for the hardness drop at the center. The fabricated AA1050/TiC composite layer was well-bonded to the aluminum substrate. TiC particles were distributed homogeneously in the FSP zone [93].

6 Repair application by FSP

For the materials which have significantly higher melting points than Al alloys, very few studies exist. Mukherjee and Ghosh [94] combined the laser-assisted direct metal deposition (DMD) with FSP for corrosion hole repair in 70/30

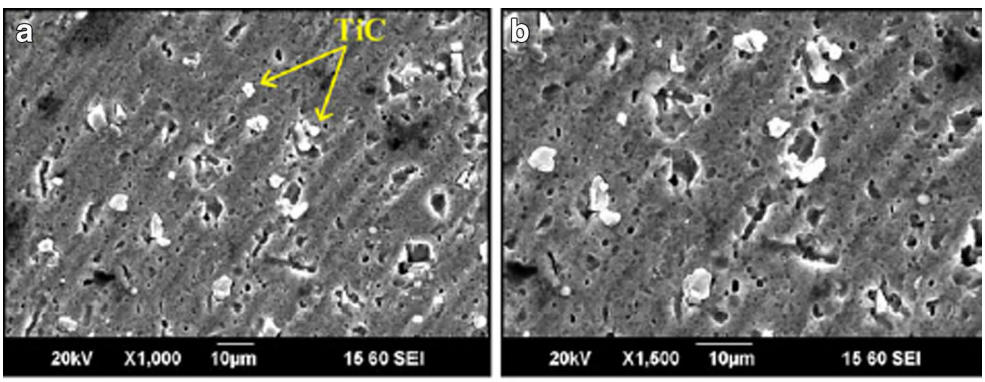

Fig. 35 **a**, **b** SEM photomicrograph of AA1050/TiC SMMC [93]

copper-nickel alloy. This additive FSP process allows for site-specific filling and repair while eliminating deleterious features of laser DMD microstructures including porosity, large grain size, residual stress, and solute segregation. Although the AFSP process as utilized in Mukherjee and Ghosh's work was not used to change chemistry, the additive Cu–Ni alloy region exhibited several benefits relative to DMD alone. The additive FSP region demonstrated higher yield and tensile strengths as well as reduced porosity from 3.3 to 0.35 % and eliminated Cu segregation typical of the DMD solidification microstructure.

7 Conclusions

From the critical analysis given previously, the following conclusions can be drawn:

FSP Friction stir-based processes can be used for welding, riveting, cladding, hardening, channeling, microstructure refining, repairing, and property enhancing.

Formability, hardness, yield strength, ductility, fracture toughness, fatigue, and corrosion resistance and surface properties of metallic materials can be improved by FSP. Aluminum, copper, magnesium, brass, plastic, and steel-based materials can be processed by FS-based processes.

Corrosion resistance of aluminum alloys can be improved by FSP. Corrosion resistance increases with the increase in the number of passes.

The tensile strength, ductility, hardness, and fatigue life of Al alloys castings can be improved by FSP due to the modification, breaking up, and homogenization of the Si needles in the eutectic phase and replacement of dendritic structure of cast to a fine equiaxed structure.

Cast iron can be surface hardened by a tool without a probe. FSP crushes and striates the graphite. Martensite structure is created by the heating the surface very locally and then cooling by a very high rate. The hardness change depends on the size of the martensite, which can be controlled by the process conditions, such as the tool traveling speed and the load. No post-surface heat treatment and no post-machining are required to obtain the required hardness, while these processes are generally essential when using the traditional methods.

For ferroalloys, on the other hand, there are limited studies concerning the hardening by FSP because of some technological barriers, such as the durability of the tool, have to be solved, although some research studies on friction stir welding have begun.

Additive FSP Incorporation of additional materials or dissimilar high melting point alloys by AFSP to locally enhance material properties/performance is a promising subject that warrants further study. FSP can be used with conjunction of additive manufacturing processes. The use of FSP in conjunction with additive manufacturing processes offers the possibility of reducing defects density, eliminating segregation, and providing grain refinement. Friction stir processing does not require filler/additive material. Hybrid processes incorporating additive methods with FSP enables local chemical composition and/or phase content to be combined with the beneficial microstructural modification of the friction stir process.

This additive process could include fusion base additive processes such as laser-engineered near net shaping (LENS), thermal spray, laser-assisted direct metal deposition, etc. Solid-state additive processes such as cold spray, kinetic metallization, or selective laser sintering (SLS) could also be utilized as additive techniques.

It can be postulated that AFSP can enable the use of high deposition rates of additive material because any cracks or discontinuities formed during deposition will be eliminated, thus increasing overall productivity.

FSP can be used in conjunction with fusion base additive processes such as laser-engineered near net shaping, thermal spray, laser-assisted direct metal deposition, and solid-state additive processes such as cold spray, kinetic metallization, or selective laser sintering to reduce defects density, to eliminate segregation, to provide grain refinement, and to improve the property of the materials.

FSP porous materials The mechanical properties of porous metallic materials such as aluminium foams can be improved by FSP. Indentation strength and energy absorption ability of porous metallic materials such as aluminum foams can be increased equivalent to about 2.2 times the value of base material by FSP. Remarkable microstructural refinement and densification can be obtained on the surface of porous materials. FSP is an effective technology in forming the dense layer near the surface of the porous metals, without any dense skin materials.

The surface region of the UZ is composed of the open pores, although the closed pores were observed in the inner region. In contrast, a very dense layer can be formed near the surface of the SMZ. Cell wall material plastically is deformed near the surface region by the high speed rotating tool during the FSP. SMZ of porous metallic materials can be formed by the localized collapse and densification of the cell structure near the surface region due to friction phenomena with the rotating tool.

FSP composite Composite layer well-bonded to the substrate can be manufactured with FSP. Surface metal matrix composites can be obtained by FSP with little or no disintegration of ceramic particles. Metal matrix composites such as Ti/SiC with microhardness values approximately 3 times greater than as-received Ti alloy can be produced by FSP. The solid-state

nature of FSP makes it an attractive method for site-specific fabrication of near-surface light metal-based MMCs. Increasing the number of pass creates a homogenous distribution of nano-sized SiC particles within the stir zone and increases the hardness of the composite.

SMMC can be produced by FSP. The FSP zone is typically about the size of the rotating pin. TiC particles reinforced composite layer well-bonded to the aluminum alloy substrate with 45 % higher hardness can be produced on the surface of the aluminum alloy.

Joining When compared with other traditional joining processes, friction stir-based joining processes presents advantages;

Mechanical benefits: Low welding distortion and good dimensional stability, low residual stress, low risk of cold cracking, improved joint strength (static and fatigue), weldability of dissimilar alloys and materials, good surface appearance, and leaner manufacturing process.

Economic benefits: Improved materials use, no waste and possibility to welding plates with different thicknesses, low energy consumption, joint weight reduction (allowing fuel consumption reduction in transportation structures), lower processing time, reliable process (low defect rate), no consumables as filler materials or shielding gas.

Environmental benefits: No shielding gases required and gases not released, lower energy consumption in the process and during service, in most of the cases, it does not require solvents for decreasing.

Nevertheless, the FSW process also presents some drawbacks and technical obstacles which might obstruct its implementation in some applications: Reaction to the process loads requires special fixture systems, access to both sides of the working pieces, the beginning of the weld usually presents lower properties, the end of the weld has the keyhole, limitations in the joint geometries, such as welding T corners, tool control (distance between the pin tip and the backing bar), root defects along the welding line, and reduction of maximum elongation at break.

Finer microstructure of weld can be obtained by FSW process due to the stirring effect. Refined structure improves the mechanical properties of the FSW joint. Better mechanical properties can be obtained with solid-state FSW than liquid phase welding processes. Low heat input, the stirring effect, and refined structure, improve the mechanical properties of the FSW joint. On the other hand, in the MIG welding process, a coarser columnar crystalline structure is obtained. A higher heat intensity in the liquid phase welding processes such as MIG deteriorates the mechanical properties of the weld joints. The results of the tensile tests of aluminum alloy show that 88 % strength improvement can be obtained by the FSW process when compared with MIG. Heat-affected zone of FSW is narrower than the MIG welded joints. Due to the less heat input, hardness reduction region of FSW is narrower than its liquid counterparts.

The parameters of FSW influence fatigue behavior of FSW joints. Parameter optimization is needed to obtain better fatigue performance of FSW joint.

In macrosections of good quality FSW welds, nugget is visible at the center of the weld. Outside the nugget, there is a thermomechanically affected zone, which has been severely plastically deformed and shows some areas of partial grain refinement

The right matching between tool and process parameters determines the final mechanical properties of the friction stir spot welding. The tool geometries remarkably determine the final welding result, according to the process parameters. Increase in the tool pin increases the tensile shear strength of FSSW.

Higher static shear strength with the ratio of 38.5 % can be obtained by RFSSW of Al alloys than that by conventional FSSW. Better corrosion resistance can be obtained by RFSSW than FSSW.

Riveting Better static and fatigue strength from the friction stir blind riveting process are obtained when compared with conventional spot welding. The quality of friction stir riveted joint relies on the rivet, the mixed zone around rivet trunk, and the solid bonding between two sheets. Mechanical properties of the FS riveted joints can be controlled by process parameters: the spindle speed, feed rate, feed depth, and the preheating time. FSR is feasible for rapid joint fabrication in volume production. Better static and fatigue strength from the friction stir blind riveting process are obtained when compared with conventional spot welding.

Formability—tailor welded blanks One of the indicators of formability of metallic materials is elongation obtained by tensile test. The elongation values of FS welds are higher than liquid base welding processes. Formability testing (LDH test) shows that the FSW is more formable than the GTAW. FSW joints have better formability characteristics than liquid phase welding processes due to its solid-state nature and refined microstructure. Due to its better formability characteristics, FSW can be effectively used to join tailor-welded blanks. The joined flat sheets can be formed into its final shape after FSW. Friction stir welding provides better ductility than gas tungsten arc welding because it causes less softening in the HAZ. The combination of single-point incremental forming with tailored welded blanks produced by FSW seems promising in the manufacture of complex sheet metal parts with high depths. SPIF of FSW tailored blanks is capable of producing industrial sheet metal parts with high-forming depths if a good quality control of the welding joints is ensured. The final quality of the sheet metal parts is greatly dependent on the quality of the welding joint produced by friction stir

welding. FSW can be used efficiently to produce and form tailored blanks.

Channeling Internal channels with any desirable path can be manufactured by FS channeling. FS channeling has the adequate potential to be introduced in the mold industry, which includes injection molding as well as open molding techniques. FS channeling can be used to produce of channels (mini channels) for the heat exchanger industry. The friction stir channels result from the application, in the visco-plasticized workpiece material, of an upward action along the threaded probe combined with an outward action along the scrolled shoulder. The FSCn process can be controlled by selecting the adequate processing parameters: tool travel speed, tool rotation speed, the size of the probe, and shoulder.

Channel shapes usually vary nonlinearly with the process parameters (the tool rotation speed and tool travel speed). Geometric features of probe influence the shape of the channel. The form of the channel can be attributed to the volume of processed material that is displaced from the base of the probe for every rotation of the tool and also the compacting force that is applied on the channel ceiling during the linear forward movement performed by the shoulder.

Cladding The friction stir cladding (FSC) technology enables the deposition of a solid-state coating using filler material on a substrate with good metallurgical bonding. Protective coating against wear and corrosion can be deposited by FSC.

Repair

Deleterious features of direct metal deposition can be repaired by using FSP with combinations of DMD. This additive FSP process allows for site-specific filling and repair while eliminating deleterious features of laser DMD microstructures including porosity, large grain size, residual stress, and solute segregation. Defects can be removed and modified. Process can be used to remove local defects and locally modify material properties, such as ductility, fatigue life, and fracture toughness. A heterogeneous microstructure can be transformed to a more homogeneous, refined microstructure.

Developments in friction stir-based processes have led to improved metallurgical and mechanical properties such as: microstructure modification, refinement, homogenization, surface cladding, corrosion, fatigue, wear, and hardness of metallic materials. The results of the study conclusively predict that reasonable costs and improved properties of processed materials will lead to a massive use of friction stir-based processes.

References

1. Mehta KP, Badheka VJ (2015) Influence of tool design and process parameters on dissimilar friction stir welding of copper to AA6061-T651 joints. Int J Adv Manuf Technol. doi:10.1007/s00170-015-7176-1
2. Threadgill PL, Leonard AJ, Shercliff HR, Withers PJ (2009) Friction stir welding of aluminium alloys. Int Met Rev 54(2): 49–93
3. Ma ZY (2008) Friction stir processing technology: a review. Metall Mater Trans A 39A:642–658
4. Carlone P, Astarita A, Palazzo GS, Paradiso V, Squillace A (2015) Microstructural aspects in Al–Cu dissimilar joining by FSW. Int J Adv Manuf Technol. doi:10.1007/s00170-015-6874-z
5. Abdolahzadeh A, Omidvar H, Safarkhanian MA, Bahrami M (2014) Studying microstructure and mechanical properties of SiC-incorporated AZ31 joints fabricated through FSW: the effects of rotational and traveling speeds. Int J Adv Manuf Technol 75: 189–196. doi:10.1007/s00170-014-6205-9
6. Xu N, Ueji R, Fujii H (2015) Enhanced mechanical properties of 70/30 brass joint by multi-pass friction stir welding with rapid cooling. Sci Technol Weld Join 20:91–99. doi:10.1179/1362171814Y.0000000261
7. Bilici MK, Yükler AI, Kastan A (2014) Effect of the tool geometry and welding parameters on the macrostructure, fracture mode and weld strength of friction-stir spot-welded polypropylene sheets. Mater Technol 48:705–711
8. Zhou L, Zhou WL, Huang YX, Feng JC (2015) Interface behavior and mechanical properties of 316L stainless steel filling friction stir welded joints. Int J Adv Manuf Technol. doi:10.1007/s00170-015-7237-5
9. Sergio MOT (2011) Design and advanced manufacturing of aircraft structures using friction stir welding, a dissertation submitted to the Faculty of Engineering of the University of Porto for the degree of Doctor of Philosophy in Leaders for Technical Industries of the MIT-Portugal Program, Porto
10. Hsieh MJ, Chiou YC, Lee RT (2015) Friction stir spot welding of low-carbon steel using an assembly-embedded rod tool. J Mater Process Technol 224:149–155. doi:10.1016/j.jmatprotec.2015.04.033
11. Thomas WM, Nicholas ED, Needham JC, Murch MG, Templesmith P, Dawes CJ (1991) G.B. Patent Application No. 9125978
12. Karthikeyan L, Senthilkumar VS, Balasubramanian V, Natarajan S (2009) Mechanical property and microstructural changes during friction stir processing of cast aluminum. Mater Des 30:2237–2242
13. Wang Y, Mishra RS (2007) Finite element simulation of selective superplastic forming of friction stir processed 7075 Al alloys. Mater Sci Eng A 2007(463):245–248
14. Elangovan K, Balasubramanian V (2007) Influences of pin profile and rotational speed of the tool on the formation of friction stir processing zone in AA2219 aluminium alloy. Mater Sci Eng 459: 7–18
15. Zhao X, Kalya P, Landers RG, Krishnamurthy K (2009) Empirical dynamic modeling of friction stir welding processes. J Manuf Sci Eng 131, 0210011-0210011-9. doi:10.1115/1.3075872
16. Woo W, Feng Z, Hubbard CR, David SA, Wang XL, Clausen B, Ungar T (2007) In situ neutron diffraction measurements of temperature and stresses during friction stir welding of 6061-T6 aluminium alloy. Sci Technol Weld Join 12(4):298–303
17. Werschmoeller D, Ehmann K, Li X (2011) Tool embedded thin film microsensors for monitoring thermal phenomena at tool-workpiece interface during machining. J Manuf Sci Eng 133(2), 021007-021007-8. doi:10.1115/1.4003616

18. Mishra RS, Mahoney WM, McFadden SX, Mara NA, Mukherjee AK (1999) High strain rate superplasticity in a friction stir processed 7075 Al alloy. Scr Mater 42:163–168
19. Ipekoğlu G, Erim S, Kıral BG, Çam G (2013) Investigation into the effect of temper condition on friction stir weldability of AA6061 Al-alloy plates. Kovove Mater 51:155–163
20. Ferraz MFS (2012) Friction stir channelling—dissertation for PHD in Mech Eng, Instituto Superior Tecnico, Universidade Tecnica de Lisboa p. 24
21. Doude RH, Haley R, Schneider JA, Nunes AC (2014) Influence of the tool shoulder contact conditions on the material flow during friction stir welding. Metall Mater Trans A 45:4411–4422
22. Mofid AM, Zadeh AB, Ghani FMM, Gur CH (2012) Submerged friction-stir welding (SFSW) underwater and under liquid nitrogen: an improved method to join Al alloys to Mg alloys. Metall Mater Trans A 43A:5106–5114
23. Kulekci MK, Şik A, Kaluç E (2008) Effects of tool rotation and pin diameter on fatigue properties of friction stir welded lap joints. Int J Adv Manuf Technol 36:877–882
24. Gungor B, Kaluc E, Taban E, Sik A (2014) Mechanical, fatigue and microstructural properties of friction stir welded 5083-H111 and 6082-T651 aluminum alloys. Mater Des 56:84–90
25. Xu VF, Liu JH, Chen DL, Luan GH (2014) Low-cycle fatigue of a friction stir welded 2219-T62 aluminum alloy at different welding parameters and cooling conditions. Int J Adv Manuf Technol 74: 209–218
26. Çam G, Mistikoglu S (2014) Recent developments in friction stir welding of Al-alloys. J Mater Eng Perform 23:1936–1953
27. Kulekci MK (2003) Mechanical properties of friction stir-welded joints of AlCu4SiMg aluminium alloy. Kovove Mater 41(2):97–105
28. Khairuddin JT, Abdullah J, Hussain Z, Almanar IP (2012) Principles and Thermo-Mechanical Model of Friction Stir Welding. In: Kovacevic R (Ed), Welding Processes, In Tech, p 191–216
29. Bozkurt Y, Salman S, Çam G (2013) The effect of welding parameters on Lap-shear tensile properties of dissimilar friction stir spot welded AA5754-H22/2024-T3 joints. Sci Technol Weld Join 18:337–345
30. Ipekoğlu G, Erim S, Çam G (2014) Investigation into the influence of post-weld heat treatment on the friction stir welded AA6061 Al-Alloy plates with different temper conditions. Metall Mater Trans A 45(2):864–877
31. Kulekci MK, Kaluç E, Şik A, Basturk O (2014) Experimental comparison of mig and friction stir welding processes for en AW-6061-T6 (Al Mg1 Si Cu) aluminium alloy. Arab J Sci Eng 35:321–330
32. Kulekci MK, Sik A (2006) Effects of tool rotation and transverse speed on fatigue properties of friction stir welded AA 1050-H18 aluminium alloy. Arch Metall Mater 51:213–216
33. Kulekci MK, Esme U, Er O (2011) Experimental comparison of resistance spot welding and friction-stir spot welding processes for the en aw 5005 aluminum alloy. Mater Technol 45:395–399
34. Yin YH, Sun N, North TH, Hu SS (2010) Hook formation and mechanical properties in AZ31 friction stir spot welds. J Mater Process Technol 210:2062–2070
35. Scotchmer N, Chan K (2012) What's new for welding aluminum in the auto industry. Weld J 91:34–37
36. Barlas Z, Ozsrac U (2012) Effects of FSW parameters on joint properties of AlMg3 alloy. Weld J 91:16–22
37. Yuan W, Mishra RS, Webb S, Chen YL, Carlsson B, Herling DR, Grant GJ (2011) Effect of tool design and process parameters on properties of Al alloy 6016 friction. J Mater Process Technol 211: 972–977
38. Kallee SW, Davenport J, Nicholas ED (2002) Railway manufacturers implement friction stir welding. Weld J 81:47–50
39. Liu F, Ma Z (2008) Effect of friction stir processing on the microstructure of as-cast 7075 aluminum alloy. Acta Metall Sin 44(3): 319–324
40. Fujii H, Cui L, Maeda M, Nogi K (2006) Effect of tool shape on mechanical properties and microstructure of friction stir welded aluminum alloys. Mater Sci Eng A 419:25–31
41. Peel M, Steuwer A, Preuss M, Withers PJ (2003) Microstructure, mechanical properties and residual stresses as a function of welding speed in aluminium AA5083 friction stir welds. Acta Mater 51(16):4791–4801
42. Tao Y, Zhang Z, Ni DR, Wang D, Xiao BL, Ma ZY (2014) Influence of welding parameter on mechanical properties and fracture behavior of friction stir welded Al-Mg-Sc joints. Mater Sci Eng A 612:236–245
43. Ahmadkhaniha D, Sohi H, Zarei-Hanzaki A (2014) Optimisation of friction stir processing parameters to produce sound and fine grain layers in pure magnesium. Sci Technol Weld Join 19:235–241
44. Fehrenbacher A, Duffie NA, Ferrier NJ, Pfefferkorn FE, Zinn MR (2014) Effects of tool-workpiece interface temperature on weld quality and quality improvements through temperature control in friction stir welding. Int J Adv Manuf Technol 71(1–4):165–179
45. Fehrenbacher A, Duffie NA, Ferrier NJ, Pfefferkorn FE, Zinn MR (2011) Toward automation of friction stir welding through temperature measurement and closed-loop control. J Manuf Sci Eng 2011(133):1–12. doi:10.1115/1.4005034
46. Simar A, Bréchet Y, Meester B, Denquin A, Pardoen T (2007) Microstructure, local and global mechanical properties of friction stir welds in aluminium alloy 6005A-T6. Mater Sci Eng A 486: 85–95
47. Zahmatkesh B, Enayati MH, Karimzadeh F (2010) Tribological and microstructural evaluation of friction stir processed Al2024 alloy. Mater Des 31:4891–4896
48. Behnagh RA, Givi MKB, Akbari M (2012) Mechanical properties, corrosion resistance, and microstructural changes during friction stir processing of 5083 aluminum rolled plates. Mater Manuf Process 27:636–640
49. Kulekci MK (2008) Magnesium and its alloys applications in automotive industry. Int J Adv Manuf Technol 39:851–865
50. Fuller CB, Mahoney MW, Calabrese M, Micona L (2010) Evolution of microstructure and mechanical properties in naturally aged 7050 and 7075 Al friction stir welds. Mater Sci Eng A 527:2233–2240. doi:10.1016/j.msea.2009.11.057
51. Miles MP, Melton DW, Nelson TE (2005) Formability of friction-stir-welded dissimilar-aluminum-alloy sheets. Metall Mater Trans A 36A:3335–3342
52. Ramulu PJ, Narayanan RG, Kailas SV (2013) Forming limit investigation of friction stir welded sheets: influence of shoulder diameter and plunge depth. Int J Adv Manuf Technol 69:2757–2772
53. Silva MB, Skjoedt M, Vilaça P, Bay N, Martins PAF (2009) Single point incremental forming of tailored blanks produced by friction stir welding. J Mater Process Technol 209:811–820
54. Muci-Küchler KH, Kalagara S (2010) Simulation of a refill friction stir spot welding process using a fully coupled thermo-mechanical FEM model. J Manuf Sci Eng 132(1), 0145031-0145031-5. doi:10.1115/1.4000881
55. Boiocchi F (2014) Friction stir spot welding applied to TP AA6061-T4 sheet metals Metalworking World Magazine. 15 March: pp. 1–5
56. Kulekci MK, Er O (2012) Determination of optimum welding parameter levels for friction stir spot welded en AW - 5005(Al Mg1) aluminium alloy. J Fac Eng Archit Gazi Univ 27(3):537–545
57. Kulekci MK (2014) Effects of process parameters on tensile shear strength of friction stir spot welded aluminium alloy (EN AW

5005). Arch Metall Mater 59:221–224. doi:10.2478/amm-2014-0035
58. Uematsu Y, Tokaji K, Tozaki Y, Kurita T, Murata S (2008) Effect of re-filling probe hole on tensile failure and fatigue behavior of friction stir spot welded joints in Al−Mg−Si alloy. Int J Fatigue 30:1956–1966
59. Shilling C, Santos JD (2002) Method and device for joining at least two adjoining work pieces by friction welding: Patent Application No. US0179682 [P]. 2002-12-05
60. Mazzaferro JAE, Rosendo TS, Mazzaferro CCP, Ramos FD, Tier MAD, Strohaecker TR, dos Santos JF (2009) Preliminary study on the mechanical behavior of friction spot weld. Soldagem e Inspecao 14:238–247
61. Venukumar S, Yalagi S, Muthukumaran S (2013) Comparison of microstructure and mechanical properties of conventional and refilled friction stir spot welds in AA 6061-T6 using filler plate. Trans Nonferrous Metals Soc China 23:2833–2842
62. LOCAL CLADDING OF ADVANCED AL ALLOYS EMPLOYING FRICTION STIR WELDING. University Twente Web. http://www.utwente.nl/ctw/tm/research/projects/FSC/ Accessed 11 September 2014
63. Rodelas JM, Lippold JC, Rule JR, Livingston J (2011): Friction stir processing as a base metal preparation technique for modification of fusion weld microstructures. In: Mishra RS, Mahoney WW, Lienert TJ (Ed) *Friction Stir Welding and Processing VI*, Minerals, Metals & Materials Society (TMS), pp. 21–36
64. Li YB, Wei ZY, Wang ZZ, Li YT (2013) Friction self-piercing riveting of aluminum alloy AA6061-T6 to magnesium alloy AZ31B. J Manuf Sci Eng 135:1–7. doi:10.1115/1.4025421
65. Ma G (2012) A thesis-friction-stir riveting, characteristics of friction-stir riveted joints. The University of Toledo, Toledo
66. Luo H (2008) New joining techniques for magnesium alloy sheets, MS thesis. Institute of Metal Research, Chinese Academy of Sciences, China, pp 48–63
67. Yang XW, Fu T, Li WY (2014) Friction stir spot welding: a review on joint macro- and microstructure, property, and process modelling. Adv Mater Sci Eng 2014:1–11
68. Ferraz MFS (2012) Friction stir channelling, dissertation for PHD. Mech Eng Instituto Superior Tecnico, Universidade Tecnica de Lisboa, Lisboa, pp 67–82
69. Nicholas ED, Thomas WM (1998) A review of friction processes for aerospace applications. Int J Mater Prod Technol 13:45–55
70. Hsu CJ, Kao PW, Ho NJ (2005) Ultrafine-grained Al–Al2Cu composite produced in situ by friction stir processing. Scr Mater 53:341–345
71. Santella ML, Engstrom T, Storjohann D, Pan TY (2005) Effects of friction stir processing on mechanical properties of the cast aluminum alloys A319 and A356. Scr Mater 53:201–206
72. Surekha K, Murty BS, Rao KB (2008) Microstructural characterization and corrosion behavior of multipass friction stir processed AA2219 aluminium alloy. Surf Coat Technol 202:4057–4068
73. Alidokht SA, Abdollah-zadeh A, Soleymani S, Assadi H (2011) Microstructure and tribological performance of an aluminium alloy based hybrid composite produced by friction stir processing. Mater Des 37:2727–2733
74. Ma ZY, Sharma SR, Mishra RS (2006) Microstructural modification of as-cast Al–Si–Mg alloy by friction stir processing. Metall Mater Trans A 37:3233–3236
75. Lee WB, Yeon YM, Jung SB (2003) The improvement of mechanical properties of friction-stir-welded A356 Al alloy. Mater Sci Eng A 355:154159
76. Shinoda T, Kawai M (2003) Surface modification by novel friction thermomechanical process of aluminium alloy castings. Surf Coat Technol 169:456459
77. Mishra RS, Ma ZY (2003) Friction stir processing: a novel technique for fabrication of surface composite. Mater Sci Eng A 341:307–310
78. Kwon YJ, Shigematsu I, Saito N (2009) Mechanical properties of fine-grained aluminum alloy produced by friction stir process. Scr Mater 49:785–789
79. Gibson LJ, Ashby MF (1997) Cellular solids: structures and properties, 2nd edn. Cambridge University Press, Cambridge
80. Ashby M, Fleck N, Wadley H, Hutchinson J, Gibson L (2000) Metal foams: a design guide. Butterworh-Heinemann, Boston
81. Banhart J (2001) Manufacture, characterisation and application of cellular metals and metal foams. Prog Mater Sci 46:559–632
82. Yi F, Zhu Z, Zu F, Hu S, Yi P (2001) Strain rate effects on the compressive property and the energy-absorbing capacity of aluminum alloy foams. Mater Charact 47:417–422
83. Eksi A, Kulekci MK (2004) Hardness and densification behaviour of copper and bronze powders compacted with uniaxial die and cold isostatic pressing processes. Metalurgija 43:129–134
84. Vilaça P, Vidal C (2011) Modular adjustable tool and correspondent process for opening continuous internal channels in solid components. National patent pending N.° 105628 T
85. Balasubramanian N, Mishra RS, Krishnamurthy K (2011) Process forces during friction stir channeling in an aluminum alloy. Int J Mater Prod Technol 211:305–311
86. Balasubramanian N, Mishra RS, Krishnamurthy K (2009) Friction stir channeling: characterization of the channels. J Mater Process Technol 209:3696–3704
87. Vidal C, Infante V, Vilaça P (2012) Mechanical characterization of friction stir channels under internal pressure and in-plane bending. Key Eng Mater 488–489:105–108
88. Filgueiras M, Soares F (2012) Friction stir channeling industrial applications- dissertation for the degree of master in mechanical engineering. Instituto Superior Tecnico, Universidade de Lisboa, Lisbon, pp 58–72
89. Shah RK, Sekulic DP (2003) Fundamentals of Heat Exchanger Design. First ed., Wiley, pp. 1–73
90. Wadekar VV (2005) Heat exchangers in process industry and mini- and microscale heat transfer. Sci Eng Tech 1:318–325
91. Fujii H, Yamaguchi Y, Kikuchi T, Kiguchi S, Nogi K (2009) Surface hardening of two cast irons by friction stir processing. J Phys Conf Ser 165:012013–012018
92. Fujii H, Ueji R, Takada Y, Kitahara H, Tsuji N, Nakata K, Nogi K (2006) Friction stir welding of ultrafine grained interstitial free steels. Mater Trans 47:239–242
93. Cui L, Fujii H, Tsuji N, Nogi K (2007) Friction stir welding of a high carbon steel. Scr Mater 56:637–640. doi:10.1016/j.scriptamat.2006.12.004
94. Mukherjee S, Ghosh AK (2011) Friction stir processing of direct metal deposited copper–nickel 70/30. Mater Sci Eng A 528:3289–3294. doi:10.1016/j.msea.2011.01.063
95. Newkirk J, Mishra RS, Thomas J, Hawk JA (2003) Friction stir processing to create surface composite. In: Advanced powder metallurgy & particulate materials. MPIF, Princeton, pp 6–60
96. Johannes LB, Yowell LL, Sosa E, Arepalli S, Mishra RS (2006) Survivability of single-walled carbon nanotubes during friction stir processing. Nanotechnology 17:3081–3084
97. Charit I, Mishra RS (2003) High strain rate superplasticity in a commercial 2024 Al alloy via friction stir processing. Mater Sci Eng A 341:290–296
98. Fujii H, Inada K, Ji YS, Morisada Y, Nogi K (2010) Design of Joint Properties by Friction Powder Processing. In: Chandra T, Wanderka N, Reimers W, Ionescu M (Ed). Zurich: Trans Tech Publications Ltd, pp. 2058–2063
99. Shamsipur A, Kashani-Bozorg SF, Zarei-Hanzaki A (2011) The effects of friction-stir process parameters on the fabrication of Ti/

SiC nano-composite surface layer. Surf Coat Technol 206:1372–1381

100. Marzoli LM, Strombeck AV, Santos JFD, Gambaro C, Volpone LM (2006) Friction stir welding of an AA6061/Al2O3/20p reinforced alloy. Compos Sci Technol 66:363–371
101. Ceschini L, Boromei I, Minak G, Morri A, Tarterini F (2007) Effect of friction stir welding on microstructure, tensile and fatigue properties of the AA7005/10 vol.%Al2O3p composite. Compos Sci Technol 67:605–615
102. Nami H, Adgi H, Sharifitabar M, Shamabadi H (2011) Microstructure and mechanical properties of friction stir welded Al/Mg_2Si metal matrix cast composite. Mater Des 32:976–983
103. Thangarasu A, Murugan N, Dinaharan I, Vijay SJ (2012) Microstructure and microhardness of AA1050/TiC surface composite fabricated using friction stir processing. Sadhana 37(5): 579–586